Extrasolar planets

Detections using the transit method

Schweighart Maria

Submitted to the

Institute of Physics

Geophysics, Astrophysics and Meteorology (IGAM)

in Fulfilment of the Requirements for the Degree

Bachelor of Science

at the

University of Graz, Austria

Matriculation number: 1311711

Supervisor: Ratzka Thorsten, Dipl.-Phys. Dr.rer.nat.

Graz, October 2016

ABSTRACT

An extrasolar planet is a planet orbiting a star other than the Sun. In the last 25 years, the search for exoplanets got the most rapidly developing field of astrophysics. More than 3300 of these worlds are currently known and the number increases steadily. Exoplanetary systems share similarities with the Solar system but also show new astonishing features like the hot Jupiters. These exoplanets are Jupiter-like but orbit in extreme proximity to their host star. Earth-based and space missions like Kepler, COROT, and WASP were initiated in order to detect more and more objects. The radial velocity method and the observation of a transit event are the most successful techniques to survey exoplanets. The observatory Lustbühel in Graz is well equipped to study transits, the passage of an extrasolar planet in front of the star's surface as seen from Earth. Five observations of such events were performed and four of them were successful. A significantly visible dip is detected in each of the measured light curves.

Author's preface and acknowledgment

As far back as ancient Greece, people have wondered about the existence of other worlds besides our Solar system in the universe. The idea of life elsewhere than our beloved home, the Earth, is deeply entrenched in the minds of men of letters. Around 300 BC, the Greek philosopher Epicurus stated: "There are infinite worlds both like and unlike this world of ours. […] We must believe that in all worlds there are living creatures and plants and other things we see in this world." (Epicurus, 341–270 BC)

Furthermore, some believers of this concept such as the medieval scholar Giordano Bruno (1548-1600) talked about the endlessness of the universe in the 16th century: "There are countless suns and countless Earths all rotating around their suns in exactly the same way as the seven planets of our system. We see only the suns because they are the largest bodies and are luminous, but their planets remain invisible to us because they are smaller and non-luminous. The countless worlds in the universe are no worse and no less inhabited than our Earth." (Piper, 2014, p. 4)

Ever since the idea of life elsewhere was born, the seed grew into an irresistible urge to improve the sensitivity of instruments and advance methods of detection and observation to search for extrasolar planets.

In my view all of the writers above once laid down to look up to the night sky, let the thoughts wander, and took a deep breath. In these situations, while seeing the twinkling stars and philosophizing about my life and problems, I sometimes wonder if there is someone else looking my way, watching our Sun. This special thrill drove me to stick my nose into astronomical books and papers about the latest achievements in this field of extrasolar planets.

The main goal of this bachelor thesis is to give a general insight of the various techniques to detect an extrasolar object and to determine the properties of the observed exoplanets. Fortunately, my supervisor Ratzka Thorsten provided access to the observatory Graz-Lustbühel where I was able to study five different transits of extrasolar planets. The available equipment allowed to track the star and to measure the flux variation. Appropriate computer programs to analyse the amount of received data were installed by the observatory as well.

At this point I would like to thank those people who helped me write this thesis. First of all, many thanks to my beloved family, my parents who raised me in a way that made me this open-minded and curious person I am today, and my siblings, Angelika and Thomas,

for their generous support in every aspect of life. I am so grateful for all the people who accompanied my way and motivated me to follow my dreams. I really do not know how to thank my supervisor Dr. Ratzka for giving me this huge opportunity to slip into the role of the scientist and helping me to sort the massive amount of data.

CONTENT

List of figures

List of tables

List of abbreviations and symbols

a	Semi-major axis of planetary system $a_* + a_P$
a_P	Semi-major axis of planetary orbit
a_*	Semi-major axis of stellar orbit
AU	Astronomical Unit, 1 AU $= 1.5 \cdot 10^{11}$ m
c	Speed of light in orbit around barycentre
d	Distance from observer
DE	Declination
(d: m: s)	(degree: minute: second)
E	East
F_1	Flux during transit
F_2	Flux without transit
G	Gravitational constant
(h: m: s)	(hour: minute: second)
i	Orbital inclination
J2000	Julian epoch 2000.0
km	Kilometer
K	Kelvin
K_*	Radial velocity curve amplitude
m	Metre
mag	Magnitude
mas	Milliarcsecond
min	Minutes
mm	Millimetre
M_{Jup}	Mass of Jupiter, $M_{Jup} = 1.9 \cdot 10^{27}$ kg
M_P	Planetary mass
M_*	Stellar mass
m_1	Apparent magnitude during transit
m_2	Apparent magnitude without transit
N	North
P	Orbiting period
pc	Parsec
R	Red bandpass filter
RA	Right ascension
R_P	Planetary radius
R_{sol}	Radius of the Sun, $R_{sol} = 6.96 \cdot 10^8$ m
R_*	Stellar radius
s	Second
UT	Universal time
v_P	Planetary speed in orbit
v_r	Radial velocity
v_*	Stellar speed in orbit around barycentre
α	Angular semi-major axis
$\Delta\lambda$	Wavelength shift
λ	Wavelength at rest
µas	Mircoarcsecond
°	Degree

1 Introduction

1.1 What is an extrasolar planet?

With the discovery of Eris, the International Astronomical Union (IAU) was forced to create new definitions for the planetary bodies found in the Solar system. Originally the word “planet” described “wanderers”, moving lights in the sky. In 2006 the IAU released the updated definition:

“A ‘planet’ is a celestial body that (1) orbits the Sun, (2) has sufficient mass for its self-gravity to overcome rigid body forces so that it assumes a hydrostatic equilibrium (nearly round) shape, and (3) has cleared the neighbourhood around its orbit.” (IAU, 2006)

As the name suggests an extrasolar planet or exoplanet is a planet orbiting a star other than the Sun. Possible nomenclatures one might come across are exoplanets, extrasolar planet, or – when the planet’s properties resemble that of a planet in the Solar system – exo-Earth, exo-Jupiter.

1.2 The way to success

By now our Solar system is known by heart in comparison to the hidden places beyond our “home”. So there is of course the desire to broaden our horizon to see if there is an Earth-like planet capable of harbouring some kind of life. Many science-fiction films and artistic interpretations put different pictures in our minds of what these worlds could look like and no limit will restrict the individual imagination. In contrast, scientists always aim to understand reality as accurate as possible. Hence the quest for the seemingly strange places was and is still driving some ambitious programmes of research.

In the mid-20th century exoplanets were set in a tighter focus. The first hints of a terrestrial object orbiting a star other than the Sun were announced at the end of the 1980s. In 1992 the existence of worlds beyond our Solar system was verified by the discovery of a planetary system around the millisecond pulsar PSR B1257+12. 1995 needs to be highlighted because the first object orbiting a solar-type main-sequence star (51 Pegasi) was measured by the Swiss astronomers Mayor and Queloz. Approximately 15 pc from Earth the gas giant 51 Pegasi b which is half the mass of Jupiter orbits its host star at a distance of 0.05 AU in just 4.2 days. The variation in the radial velocity revealed the planet. For years the radial velocity method was the only one to provide reasonable results. However, this planet does not offer the necessary surface conditions to support some form of life. Taking the star’s properties and the separation between both objects, the surface temperature is estimated to be 1250 K. That is why exoplanets like this one are called “hot Jupiters”. (Piper, 2014, p. 24-28)

Just after the first detection, things then started to move at a rapid pace. After centuries of philosophical speculation this breaking news encouraged other researchers to continue their hunt for extrasolar planets. Not until 1999 the very first transiting planet was observed. Research groups all around the globe are vibrantly involved in a vast network of both observational and theoretical aspects. Figure 1 shows the explosive increase in detections since the first exoplanet was found in 1989 (NASA Exoplanet Archive, 2016). A growing fraction of exoplanets is detected by transits in front of the host star as seen from Earth. Predominantly due to the Kepler mission thousands of alien worlds were detected, set as candidates, or/and later confirmed.

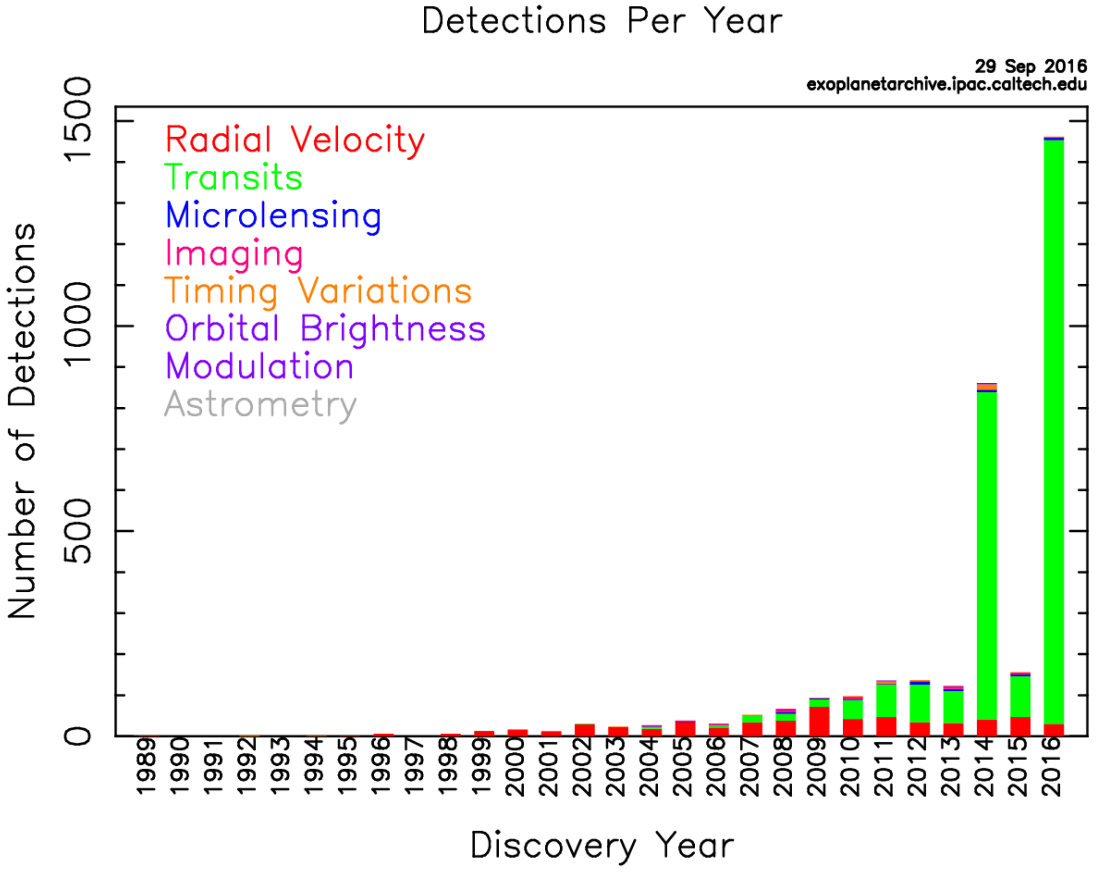

Figure 1: Evolution in number of discoveries. (NASA Exoplanet Archive, 2016)

1.3 How many are there?

The NASA Exoplanet Archive collects and provides public data to support the search and characterization of extrasolar planets and their host stars. As of September 29th, 2016, 3394 confirmed exoplanets were listed in this database. So far the majority of host stars are orbited just by one planet, the others form 573 multi-planet systems. Table 1 presents the number of confirmed extrasolar planets detected by using the indicated method (NASA Exoplanet Archive, 2016). These techniques will be discussed in particular in

Chapter 2. The transiting exoplanets constitute with about 80 % the majority of all confirmed objects.

Table 1: Confirmed exoplanets statistics. (NASA Exoplanet Archive, 2016)

Discovery method	**Number of planets**
Astrometry	1
Imaging	43
Radial velocity	597
Transit	2677
Transit timing variations	15
Eclipse timing variation	8
Microlensing	40
Pulsar timing variations	5
Pulsation timing variations	2
Orbital brightness modulation	6
Transiting exoplanets	2701
Total	3394

In 2009 the space observatory Kepler was launched by NASA, which is designed to discover Earth-size and smaller planets in or near the habitable zone of other stars in our neighbourhood of the galaxy and survey billions of stars that might have such planets. Table 2 quantifies the success of this program (NASA Exoplanet Archive, 2016). About 70 % of all confirmed planets were detected by Kepler and over 2000 objects are marked as candidates. Those will be further investigated.

Table 2: Kepler mission. (NASA Exoplanet Archive, 2016)

Confirmed planets	2330
Candidates and confirmed in habitable zone[1]	297
Kepler project candidates [2]	4696
Kepler project unconfirmed candidates	2416
Total (confirmed and unconfirmed)[3]	4746

1.4 Observatories for exoplanet transits

As mentioned before, the Kepler mission by NASA is the most successful project in this context. 2330 out of the 3394 confirmed alien planets, which is approximately 70%, are known due to this survey (Kepler, 2016). Another mission, WASP (Wide Angle Search for Planets), is the UK's leading extrasolar planet detection programme which has examined over 100 stars and is located in La Palma (WASP, 2014). 29 planets are named after the space telescope COROT which is an acronym for "convection, rotation and planetary transits". Besides the search for exoplanets, the program was also designed to detect and

[1] 180 K < equilibrium (T) < 310 K or 0.25 < insolation (earth flux) < 2.2
[2] All planets that have ever been marked as a candidate
[3] Total candidates and confirmed planets. Some were never designated as candidates.

study stars’ vibrations (stellar seismology). This space observatory mission led by the French Space Agency CNES in cooperation with others ended in 2012 (COROT, 2016). The Hungarian-made automated telescope network (HATNet) has detected 57 planets since 2003. These telescopes are geographically distributed in order to be able to monitor all parts of the sky at any time. Most of the telescopes are fully robotic and make self-acted decisions on what to obverse at which time (HATNet, 2015).

The instruments of all the listed projects are especially designed to detect a periodic dim in the stellar flux. The short dip in the light curve of the observed star might be caused by a planetary-sized object moving in front of the star. Therefore, the telescopes are optimized for detecting transiting extrasolar planets. Many more either ground- or space-based exoplanet research programmes are currently using this successful method: OGLE, TrES, XO and K2 just to name a few of them. The increasing interest in exoplanets requests for numerous missions to come. CHEOPS should be ready to be launched in 2017 with the goal to provide detailed information about the formation and the properties of the objects. (Piper, 2014, chapter 2)

1.5 How to name them all

Exoplanet detection is a fast-moving aspect of astronomy and with the help of the Kepler mission, just to mention one amongst a lot of other projects (see Chapter 1.4 for more information), many more detections are yet to come. Listing all the planets in our Solar system is a walk in the park, one learns these eight names from scratch. All of them are named after Roman gods apart from Uranus (Greek mythology). Also some satellites or other objects in our Solar system bear the names of famous classic characters. It seems like there might be no more left to describe more than 3000 extrasolar planets. What is more is that this procedure is quite time consuming in times of an inflationary rise in detections. The solution to this problem is simple: Planets discovered by earth-based or space telescopes are named after the mission and ordered chronologically. For instance, Kepler 22b is the first planet in the 22nd system with planets detected by the Kepler observatory. The first planet spotted in a system is indicated by the letter b, the second with c and so on. Others are given the host star’s label and a lower-case letter in order of discovery like 61 Vir b. Planets are never called “a”. One of Kepler's stars, Kepler 11, has been found to have six planets orbiting it, therefore the last one is called Kepler 11g. However, the IAU asked the general public to name planetary systems and their planets in the public outreach event “NameExoWorlds” (http://nameexoworlds.iau.org/).

1.6 Exoplanet types

The found extrasolar planets are classified according to the categories below. Of course subdivisions or intermediary groups are created to describe the object in greater detail but for now the listed types are sufficient to get a satisfactory idea of the planets´ properties. (Piper, S., 2014, p. 81-89, adapted from Lammer, H. et al., 2009)

1.6.1 Terrestrial planets

Features like mass, radius, and atmosphere are similar to those of the Earth. These "exo-Earths" are located in the habitable zone of the parent star allowing water to appear in its liquid form. For scientists these ones are like the holy grail because their conditions are most likely to support life. The detection of those rocky planets is, however, difficult for the transit method due to the fact that exo-Earths are quite small, approximately 10000 km in diameter. Their low mass causes also no large radial velocity modulation. That is why only a few have been found yet.

The term "super" in "Super Earths" merely indicates the planet's mass which can go up to 10 times the mass of our Earth. Despite this fact they show a rocky surface and an atmosphere that could be analysed by spectral methods during a transit. For these small planets it is even hard to tell if there is an atmosphere or not.

Entirely water covered planets are called water worlds. Not yet discovered, these exoplanets are believed to have been built out of ice and rocks in the outer zone of the young planetary system. During their inward migration they heat up and the ice melts.

1.6.2 Gas giants

Examples of this exoplanet type are even found in our Solar system: Jupiter and Saturn. Neptune and Uranus are obviously counted as gas giants but sometimes referred to as ice giants because they contain larger fractions of heavier materials like methane and ammoniac. If Jupiter had collected 80 times more material during its formation process in the protostellar cloud, it would have become a star. The process of nuclear fusion of hydrogen is required for this title. A gas planet's mass is mostly composed of hydrogen and helium with potentially a dense rocky or metallic core. The mass' minimum for gas giants is set to be 10 times the Earth's mass.

Planets that are similar in mass to Jupiter and are orbiting the parent star in direct proximity within a few days are called hot Jupiters. The term "hot" referrers to surface temperatures significantly higher than the one on Jupiter. Furthermore, the short distance causes a tidal locking which means that one side of a planet always faces the star. This effect is also known as synchronous rotation or captured rotation. Hot Jupiters show orbits with a low eccentricity and are easy to detect with the radial velocity and the transit method. That is why most of the discovered planets are members of this category. As well as objects of other types, hot Jupiters are believed to have migrated towards the central star after their formation.

Very hot Jupiters have to deal with even more extreme circumstances than hot Jupiters. They orbit much closer than Mercury around our Sun. The object OGLE-TR-56 which is about the mass of Jupiter orbits its host star in 1.2 days at a distance of 6000 km. Additionally, the extreme proximity causes even higher temperatures giving the planets a good “roast”. These planets have to be formed in the outer zone of the system because so close to the star, there could not have been enough material. Numerous theories try to explain this migration phenomenon and the involved forces but that represents a whole new issue in the exoplanet research which will not be covered in this thesis.

Figure 2 significantly shows concentrations of Jupiter-mass objects orbiting the parent star with semi-major axes around and even below 0.1 AU (NASA Exoplanet Archive, 2016).

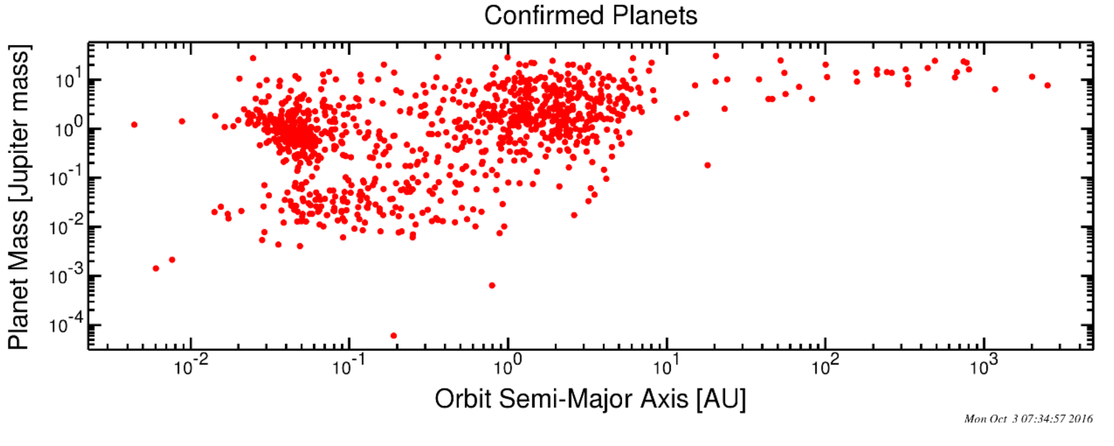

Figure 2: Jupiter-mass objects in proximity to host star. (NASA Exoplanet Archive, 2016)

Planets of this category “hot Neptune” are similar in mass and density to Neptune or Uranus but have orbits with radii of less than 1 AU. That is why they show a warmer atmosphere. Again, they should have been formed in the outer disk and then migrated inwards.

So-called Chthonian planets were originally gas giants like hot Jupiters. They moved far too close to the central star and their H/He envelope was stripped away, leaving only the rocky or metallic cores. The remnants resemble terrestrial planets.

1.6.3 Eccentrics

Great eccentricity of the orbit is the main property of these extrasolar planets. As a result, the surface temperature varies dramatically during an orbit. The objects HD 20782 b and HD 80606 b even show an eccentricity of e = 0.97, 0.93, respectively.

1.6.4 Free-floaters

These orphan planets are quite intriguing due to the fact that they do not orbit a star. Rogue planets, as they are referred to as well, are free-floating in the galaxy. It is believed that they either have somehow been ejected from the developing star system or have formed early in the Universe and have never been bound to a star (ESO 1245, 2012).

1.7 Comparison to the Solar system

Some features of the exoplanetary systems are shared with our home system. Most of the stars hosting planets are main-sequence stars similar to the Sun because solar-type stars are primarily observed. The majority of the confirmed extrasolar planets are the Jovian planets. Only a limited number of terrestrial planets has been found yet. A reason for that is the fact that detection methods are designed to look for massive bodies orbiting close to the host star. About 360 planets possess a radius smaller than 1.25 Earth radius and 28 resemble the Earth in mass (NASA Exoplanet Archive, 2016).

Most exoplanets are gaseous similar to gas giants made of hydrogen and helium gas. Others show a rockier, Earth-like composition. The so-called hot Jupiters are similar in mass to Jupiter and some orbit their parent star even closer than Mercury orbits the Sun. Theory does not allow massive objects to form in proximity to the central star. That is why it is believed that those hot Jupiters have been formed in an outer zone of the system and migrated inwards. (Perryman, 2011, p. 237-238)

Indicated by the agglomeration of red dots in the upper right area of Figure 3, it is clearly visible that most of the confirmed exoplanets show similar properties to Jupiter with regard to mass and radius (NASA Exoplanet Archive, 2016).

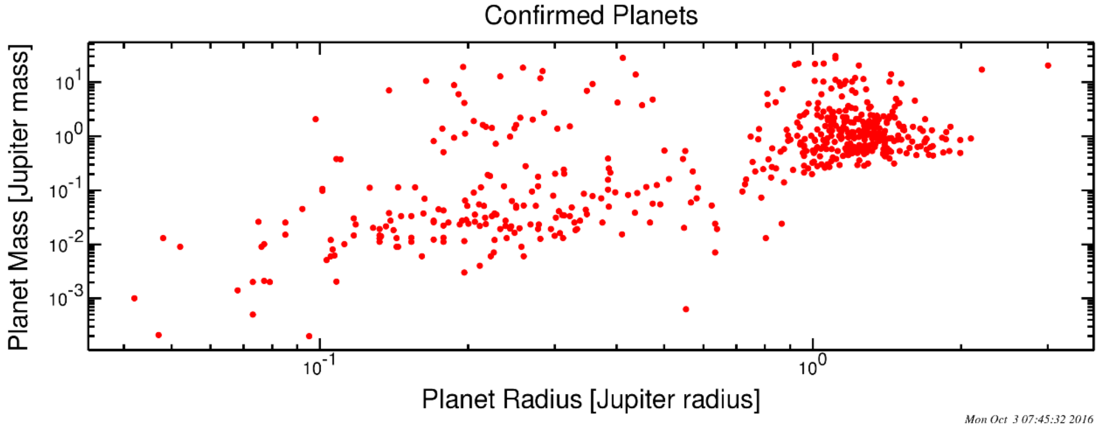

Figure 3: Jupiter-like planets. (NASA Exoplanet Archive, 2016)

Figure 4 shows that most planets have a nearly circular orbit. For exceptional cases see chapter 1.6.3 (NASA Exoplanet Archive, 2016).

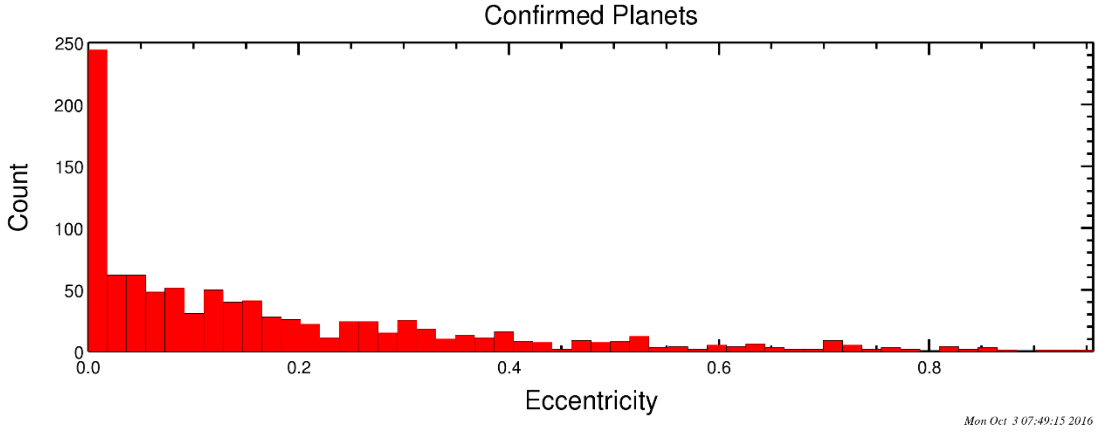

Figure 4: eccentricity. (NASA Exoplanet Archive, 2016)

2 Detection methods

In order to discover and observe an extrasolar planet, more precise and powerful instruments and sophisticated techniques need to be used. It was not until NASA's mission New Horizons in 2015 that a high quality picture of the dwarf planet Pluto at the outer edge of our own Sol system was taken. How can it be possible to detect an exoplanet much further away from Earth? The Earth's atmosphere limits the accuracy of the observations in addition. To eliminate diffraction and scattering in the atmosphere space observatories were installed. The methods to overcome the difficulties of detecting extrasolar planets are divided in direct and indirect techniques.

Taking actual images of the planet (all planets outside the Solar system stay unresolved, anyway) or extracting the planet's electromagnetic spectrum, which tells scientists about the atmospheric composition, falls under the category of direct methods. Directly observing exoplanets is very challenging, not only because of the interstellar distance but also because the star's brightness blinds the instrument used to detect the much fainter planet. The investigation is made even more difficult by the fact that the angular separation between the planet and its host star is generally small.

The three most commonly used methods (radial velocity, astrometry, transit) are referred to as indirect. Instead of detecting the planet itself its effects on the host star are recorded as a proof for the planet's existence. Both planet and star orbit around the common centre of mass. On the one hand the central star's motion can be influenced by the planet (radial velocity, astrometric method), on the other hand the star's light can be slightly dimmed by a transiting object (transit method). Gravitational lensing and pulsar timing are also indirect detection methods. (Mason, 2008, p. 2)

2.1 Radial velocity measurements

In the Solar system it seems like the Sun represents the centre of mass because it is enormously massive compared to the planets. In reality all bodies orbit a common centre of mass located inside the Sun's surface. Due to the gravitational pull of the planet(s) stars wobble around this barycentre causing the light spectrum to shift. The radial velocity method records these periodic Doppler shifts in the stellar spectrum in order to examine the properties of the exoplanetary system. If the star moves toward the observer on Earth, the light emitted has a shorter wavelength and the absorption lines are blue shifted (negative radial velocity). A red shift occurs when the star is drifting away from Earth causing a longer wavelength (positive radial velocity). There will be no shift if the star is moving perpendicular to the line of sight. Just a periodic shift in frequency indicates the presence of one or even more planets. For ground-based observatories the limiting value for this Doppler shift is about 1 m/s.

This procedure is most efficient for massive planets in proximity to smaller host stars because of the stronger gravitational pull of the planets (cf. hot Jupiter). Both the star and the planet orbit the centre of mass which includes that the objects' centre must be on different sides of the barycentre at any time. This results in the fact that the star orbits in the same time as the planet does. Concluding, the period of the planet is obtained by determining the period of the radial velocity curve of the star. Furthermore, if the mass of the planet increases, the radius of the star's orbit around the barycentre gets larger. As it still takes the same amount of time to complete an orbit the star has to move faster which is indicated by a higher amplitude of the radial velocity curve.

Relevant equations to describe this method are given below (Waldmann, 2014). The definition of all used parameters can be found in the list of abbreviations and symbols on page 13. By determining the shift in wavelenght compared to the wavelength at rest, the radial velocity is obtained as follows:

$$\frac{\Delta\lambda}{\lambda} = \frac{v_r}{c} \tag{1}$$

For the system planet – star the conservation of momentum applies:

$$M_* v_* = M_P v_P \tag{2}$$

Kepler's third law sets the semi-major axes in relation to the bodies' mass:

$$a^3 = \frac{G(M_* + M_P)}{4\pi^2} P^2 \tag{3}$$

$$a_* = \frac{M_P}{M_* + M_P} a \tag{4}$$

The stellar speed due to the gravitational pull of the planet is calculated with the following formula:

$$v_* = \frac{2\pi a_*}{P} \xrightarrow{(4)} v_* \simeq \frac{2\pi a M_P}{P M_*} \tag{5}$$

This leads to a radial velocity curve amplitude $K_* \simeq v_* \, sin(i)$.

In the early days of extrasolar planet research the radial velocity method was responsible for the majority of the discovered bodies. The first "Jupiter-mass companion to a solar-type star", as their article is called, was detected by Mayor and Queloz in 1995 using this technique. Figure 5 shows the obtained radial velocity curve of 51 Peg (Mayor & Queloz, 1995, p. 357). As of mid-2016, nearly 600 planets are identified that way (NASA Exoplanet Achieve).

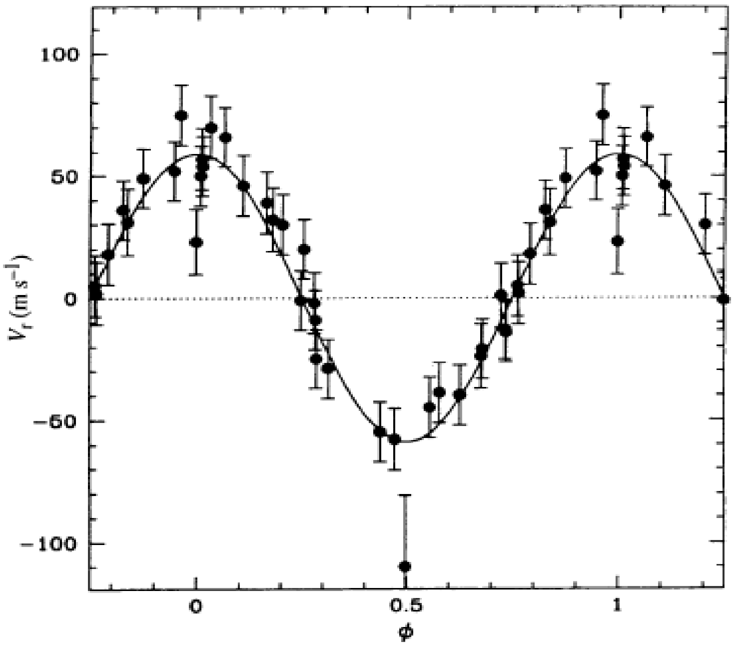

Figure 5: Orbital motion of 51 Peg. (Mayor & Queloz, 1995, p. 357)

2.2 Astrometry

The astrometric method is designed to record the transverse component of the periodic motion of the parent star around the barycentre induced by the gravitational pull of the orbiting planet. In contrast, the radial velocity technique measures the displacement along the line of sight. A series of high accuracy observations of the angular position of the star is needed to obtain an evidence of the existence of an exoplanet. Until now only one planet was detected and confirmed. But this planet was already known by other detection methods. The wobbles are simply too small to be routinely recorded by the current optical systems.

The motion of the star orbiting the barycentre projected on the plane of the sky appears as an ellipse with angular semi-major axis α:

$$\alpha = \frac{M_P}{M_* + M_P} a \simeq \frac{M_P}{M_*} a \equiv \left(\frac{M_P}{M_*}\right)\left(\frac{a}{1\ AU}\right)\left(\frac{d}{1pc}\right)^{-1} arcsec \qquad (6)$$

The planet's mass can be neglected because of the small contribution compared to the star's mass. The farther the exoplanetary system is located away from to the observer, the higher is the minimal detectable planetary mass. Astrometry is most effective for a massive planet orbiting at a large separation from the star because this leads to large semi-major axes of the apparent motion of the star. The method thus favours long orbital periods. But long orbits require long-term monitoring. (Perryman, 2011, p. 62-63)

ESA's space astrometry mission Hipparcos achieved an accuracy of about 1 mas while its operation till 1993. Currently, the best precision of about 20 µas is provided by ESA's mission Gaia which is a wide-angle survey observing about a billion stars in our galaxy. The Keck telescope as a ground-based observatory also offers accuracy at this scale. The discovery of an Earth-mass planet at a distance of 10 pc orbiting a Sun-like star at 1 AU requires submicroarcsecond precision. By now only one confirmed planet has been found by astrometry.

2.3 Transit method

Transit events are well known from our own Solar system (Venus, Mercury). This indirect observational technique detects the periodic dimming of the star's brightness due to an exoplanet transiting in front of the star's disk as seen from Earth. This temporary decrease of the starlight's intensity provides information about the extrasolar planet's and the host star's properties. The dip in intensity is of the order of 1 %. What is absolutely necessary for the application of this method is an orbital inclination close to 90 °.

Figure 6 shows the schematic transit of a planet. The corresponding light curve is indicated by the red line (Adapted from Deeg, 2002).

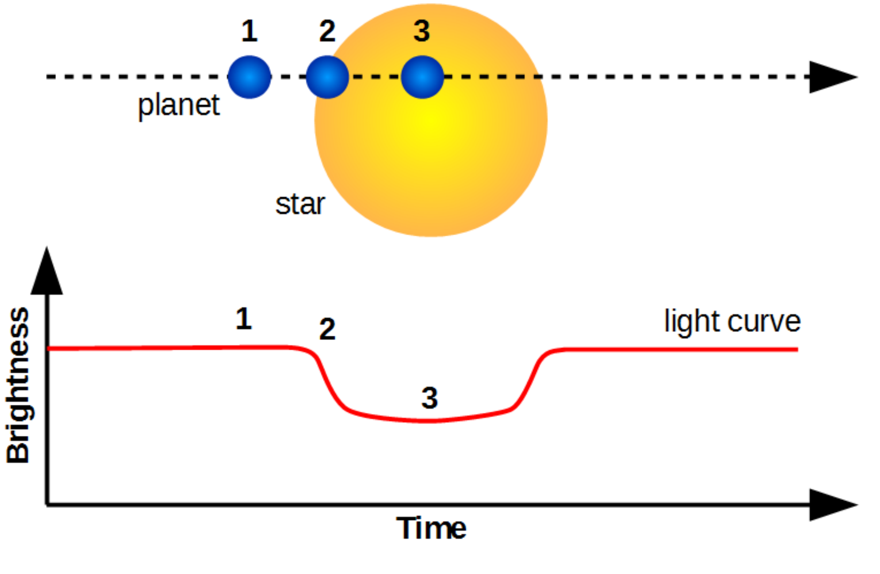

Figure 6: Schematic light curve of a transit event. (Adapted from Deeg, 2002)

The orbiting period is determined by the time span between two transit events. Kepler's third law relates the period P to the semi-major axis of the orbit a and the total mass of the objects ($M_P + M_*$):

$$\frac{a^3}{P^2} = \frac{G(M_* + M_P)}{4\pi^2} \tag{7}$$

As mentioned above the transit light curve acts instructively with respect to the characterization of the planet. The change in flux ΔF relative to the stellar flux F prior to the transit can be written as:

$$\frac{\Delta F}{F} = \frac{R_P^2}{R_*^2} \tag{8}$$

In Figure 7 the projected separation between the centre of the stellar and the planetary disk at mid-transit is introduced as the impact parameter b (adapted from Cowley & Hughes, 2014, following Haswell, 2010):

$$b = \frac{a \cdot \cos(i)}{R_*} \tag{9}$$

The transit is completed after the passage of the distance 2 l as shown in Figure 8 (adapted from Cowley & Hughes, 2014, following Haswell, 2010).

$$2l = 2\sqrt{(R_P + R_*)^2 - (bR_*)^2} \tag{10}$$

For the triangle A, B and the centre of the star, indicated in Figure 9, the following equation applies (adapted from Cowley & Hughes, 2014, following Haswell, 2010):

$$\sin\left(\frac{\alpha}{2}\right) = \frac{l}{a} \tag{11}$$

When combining the equations above, the duration of a transit t is given by:

$$t = P\frac{\alpha}{2\pi} = \frac{P}{\pi}\sin^{-1}\left(\frac{l}{a}\right) = \frac{P}{\pi}\sin^{-1}\left(\frac{\sqrt{(R_P + R_*)^2 - a^2\cos^2(i)}}{a}\right) \tag{12}$$

A circular orbit is assumed leading to an arc length of αa between A and B as the entire orbit is 2πa. (Cowley & Hughes, 2014).

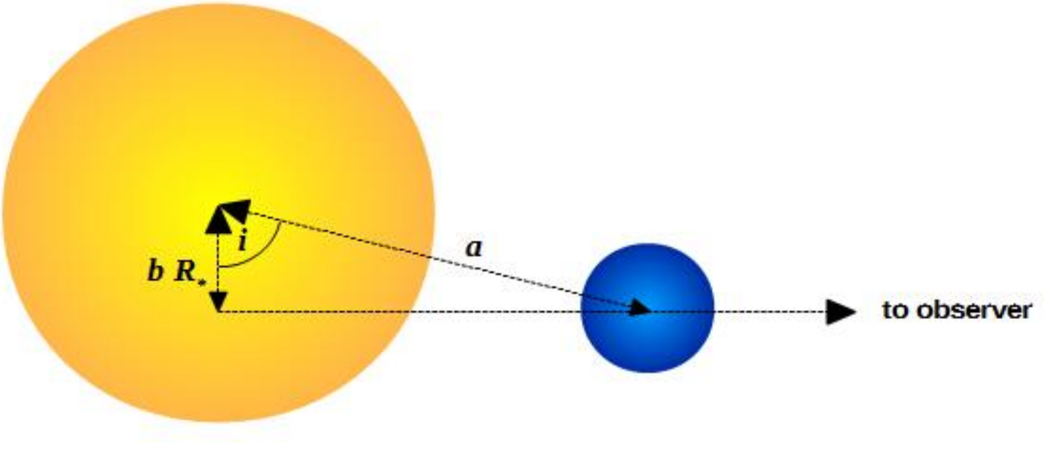

Figure 7: Impact parameter (Adapted from Cowley & Hughes, 2014, following Haswell, 2010).

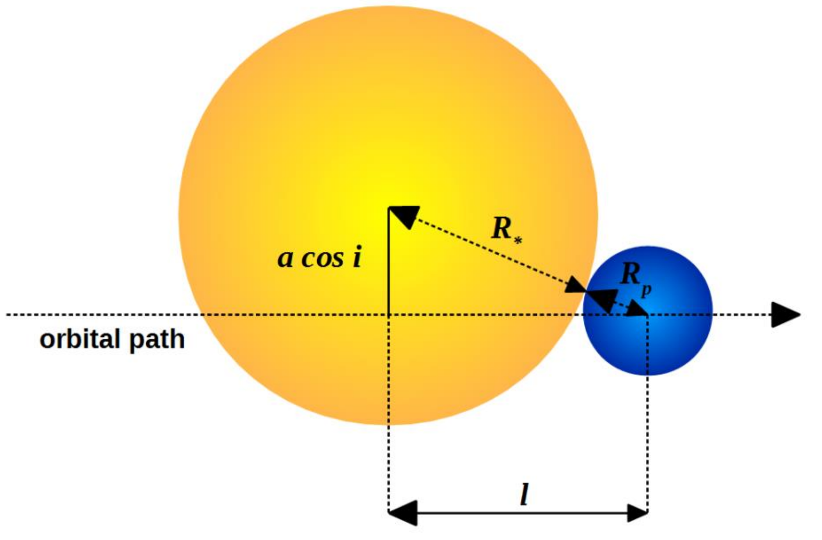

Figure 8: Transit length (Adapted from Cowley & Hughes, 2014, following Haswell, 2010).

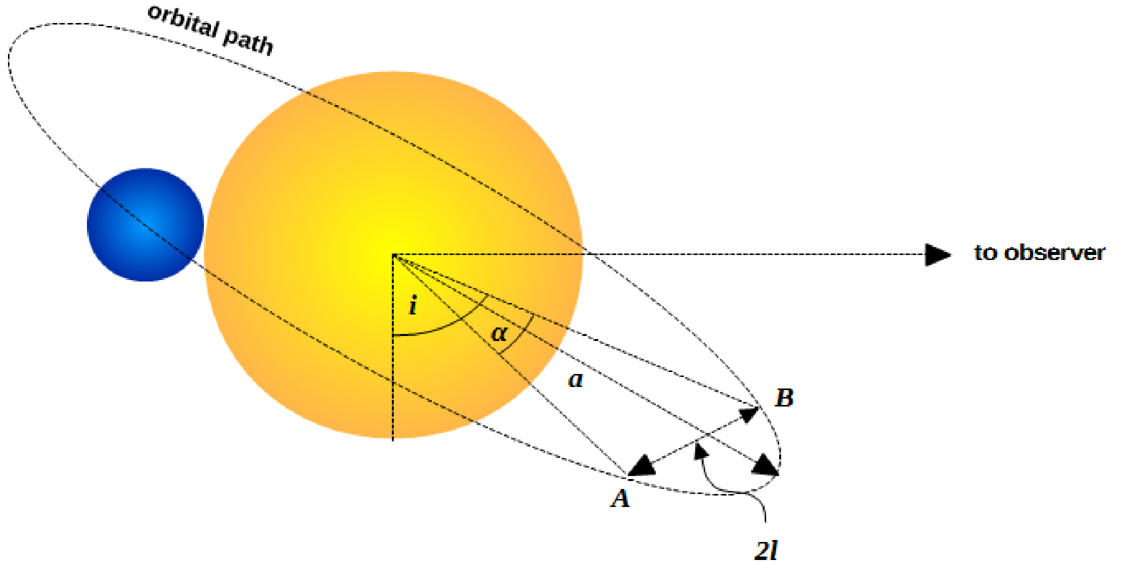

Figure 9: Geometry referring to transit duration (Adapted from Cowley & Hughes, 2014, following Haswell, 2010).

By measuring the depth and the duration of the transit, the planetary radius and the orbital inclination can be obtained. Furthermore, the true mass of the extrasolar planet will be calculated when taking the minimal mass of the planet $M_P \cdot \sin(i)$, as known from the radial velocity method, into consideration. The density is then derived as $\rho_P = \frac{3M_P}{4\pi R_P^3}$ (Cowley & Hughes, 2014).

To sum up, planetary transits allow the characterization of the planet in terms of radius, orbital inclination, and orbital period. If the mass is known from the use of, for example, the radial velocity method, it is easy to calculate the planet's density. Even atmospheric features are subject of modern research due to the absorption of starlight in the planet's atmosphere during a transit.

The detection of transiting extrasolar planets has been a huge success since the first confirmed planet detected with this method in 1999. As of mid-2016 more than 2600 transiting exoplanets are discovered and they represent about 80 % of all confirmed bodies. The majority of them were found by NASA's Kepler mission (NASA Exoplanet Archive).

2.4 Gravitational lensing

The bending of light by gravity is a fascinating aspect of general relativity. Electromagnetic waves coming from a distant background object (source) are bent by the gravitational potential of a foreground body (lens) when passing near it to reach the observer. The image of the source is distorted and appears temporarily magnified. The brightness of the source in- and decreases as the lensing object passes in front of the source. The gravitational field of an accompanying planet to a passing lensing star can lead to an additional amplification of the source images which means that star and planet act together as a multiple lens. (Perryman, 2011, p. 83-84)

The observation of a microlensing event not merely tells about the presence of a planet and magnifies the starlight coming from a distant source, but also represents the only way to detect free-floating objects. The method is responsible for the discovery of 40 extrasolar bodies (NASA Exoplanet Archive).

In Figure 10 the received light curve of a microlensing event is displayed in order to get an impression of the additional amplification of the source image (Beaulieu, J.-P. et al., 2006).

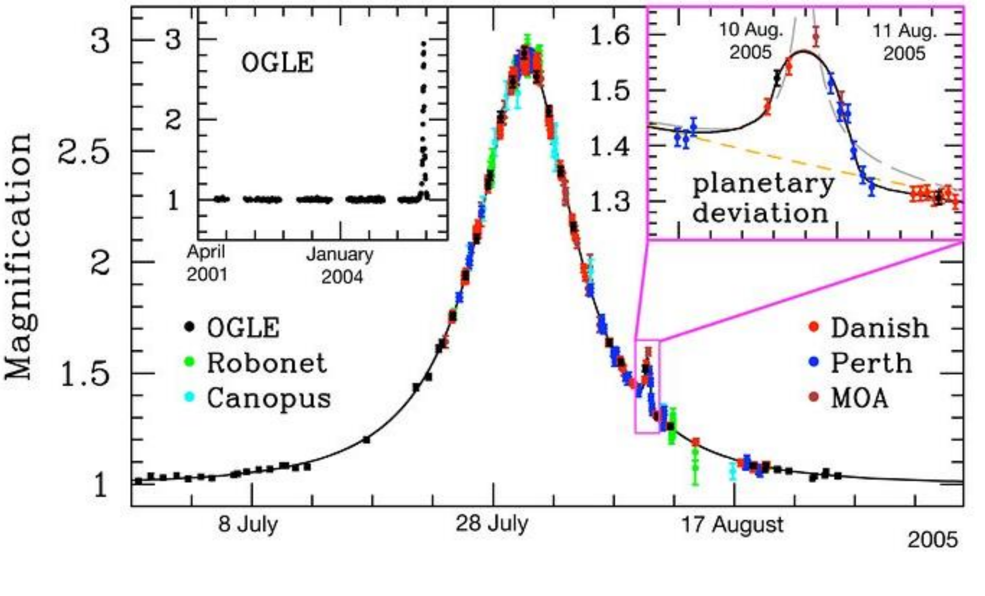

Figure 10: Light curve of a microlensing event OGLE-2005-BLG-390. (Beaulieu, J.-P. et al., 2006)

2.5 Pulsar timing

A rapidly spinning neutron star with a strong magnetic field is called a pulsar. As they rotate and their spin axis is not identical to the orientation of the magnetic field axis, pulsars emit intense electromagnetic pulses regularly. These extremely precise and stable pulses are recorded on Earth. Once again the star's motion around the barycentre of the system caused by the presence of an extrasolar planet represents the starting point of the timing method. If the pulsar is moving away from the observer when orbiting the centre of mass, the time between each pulse becomes longer and vice versa the movement towards the Earth results in shorter intervals. By precisely measuring the variations in pulse timing scientists are able not only to deduce the existence of an exoplanet, but also the orbit and the mass of the object. Pulsar timing is capable of recording Earth-mass and even smaller bodies. (Perryman, 2011, p. 75)

In 1992 the pulsar timing method was used by Wolszczan and Frail to detect the very first exoplanet around the millisecond pulsar PSR B1257+12. This planet shows the lowest exoplanetary mass of just 0.02 Earth mass. (Wolszczan & Frail, 1992)

3 Observation

3.1 Observatory Graz - Lustbühel

Since its establishment in 1976 the observatory Lustbühel located at the eastern outskirts of Graz has served as a venue of research in the fields of astronomy and telecommunications managed by the University of Graz, University of Technology Graz, and the IWF (Space Research Institute in Graz, Austrian Academy of Sciences ÖAW) (Observatory Lustbühel, 2016). The observatory's geographic coordinates are 47.0677839 N / 15.4937761 E. The elevation of the observatory is 484 m.

3.1.1 Equipment

The used instrument to observe the exoplanetary systems is the "500 mm f/9 Cassegrain Telescope" made by ASA. This optical device is of the Cassegrain type, featuring a parabolic primary mirror with a central hole and a hyperbolic secondary mirror. In order to focus the secondary mirror can be moved along the optical axis of the telescope. The mirrors are manufactured from Sitall which is a crystalline glass-ceramic showing an ultra-low coefficient of thermal expansion. Controlled by computers, the telescope can be easily used for observation programs and in combination with a CCD detector produces high quality images. The telescope has an aperture of 500 mm. A focal ratio of f/9 for a focal length of 4500 mm leads to a field of view of 61 arcminutes (ASA Cassegrain Telescope, 2016). The field of view provided by the camera is about 14' x 11'.

The attached CCD camera by SBIG is the STF-83000M model based on Kodak's KAF-8300 image sensor. The full frame CCD has 8.3 megapixel (3326 x 2504) providing linearity up to approximately 50000 counts. An integrated shutter can be closed for dark frames (SBIG CCD detector, 2014). A 2x2 binning was mostly used. The term "binning" refers to the combined read out of several pixels into a single one. For example, a 3x3 binned image indicates the merging of 9 pixels to one. This process offers advantages by reducing the amount of data, improving the signal-to-noise ratio, and speeding up the readout. During operation the CCD sensor was cooled to about 263 K in order to reduce thermal noise.

3.1.2 Data analysis

In order to handle and analyse the amount of data recorded the programming language IDL (Interactive Data Language) was utilised. The observatory provided a proprietary program ideal for astronomical data reduction. For displaying the images, the program SAOImage DS9 was installed. The analysis was again done with IDL programs that made use of NASA's IDL routines.

Depending on exposure time and temporal length of the transit, a comparatively large amount of images was taken that needed to be sorted. In order to do the reduction, the bias was subtracted, the resulting images were divided by the flat field and the bad pixels were removed. After that the science target as well as the calibrator stars were cut out separately in smaller frames resulting in a "movie" of the stars in the course of the transit event. The stars' integrated fluxes in this field of view were derived by aperture photometry. By comparing the flux of the planet's host star with the fluxes of the calibrators, the transit's light curve was generated.

3.1.3 Observation routine

Approximately one hour before the predicted starting time the instruments were put into operation and functional tests were performed. With the equatorial coordinates as an input the telescope was pointed automatically towards the science target. However, the pointing was optimised manually. Samples were generated to optimise also binning and exposure time. Half an hour before the predicted start of the transit, a series of exposures was initiated which was stopped approximately half an hour after the predicted end of the transit. The extra time before and after the predicted transit was added in order to make sure that the whole transit is captured. While the images were taken automatically, the count rate of the stars and tracking of the dome were permanently checked. If necessary, corrections were applied by changing the exposure time or moving the dome. Afterwards, dark and bias frames were taken and the instruments were shut down.

3.2 WASP-104 b

On March 18th, 2016 the transiting exoplanet WASP-104 b located in the constellation Leo was the first object to be observed. This hot Jupiter orbits in 1.755 days at a separation of merely 0.029 AU. The Sun-like parent star found at a distance of 143 pc only hosts one planet. WASP-104 b has (1.272 ± 0.047) Jupiter masses. (NASA Exoplanet Archive, 2016)

Tables 3-7 specify in greater detail the transiting extrasolar planet and give more information about the observations and the transits themselves. RA and DE (see list of abbreviations and symbols) indicate the position of the host star in the equatorial coordinate system. Its magnitude in the V-band (visual) and decrease in magnitude due to the transiting planet, indicated by the depth, are also given. Details about the duration of the transit as well as the predicted start and end are offered by the Exoplanet Transit Database (ETD). Start and end of the observation were added to the table and correspond to the axis label of the obtained light curve. The elevation describes the angle between the object in the sky and the horizon which varies during the observation. For optimal results the exposure time, focus and binning needed to be adjusted prior to the start of the observation. In some cases, the exposure time had to be modified during the observation due to the in- or decrease in the count rate. For all five transits the red bandpass filter was used.

Table 3: Event data WASP-104 b (ETD, 2016)

Name	WASP-104 b (Leo)
RA (J2000)	10:42:24.61 (h:m:s)
DE (J2000)	+ 07:26:06.3 (d:m:s)
Magnitude	11.12 mag
Depth	0.0158 mag
Duration	105.72 min
Predicted start	20:15 UT
Predicted end	22:01 UT
Start of observation	19:43 UT
End of observation	22:33 UT
Elevation	(46-51) °
Exposure time	0.5 min
Focus	4.25 mm
Filter	R
Binning	2x2

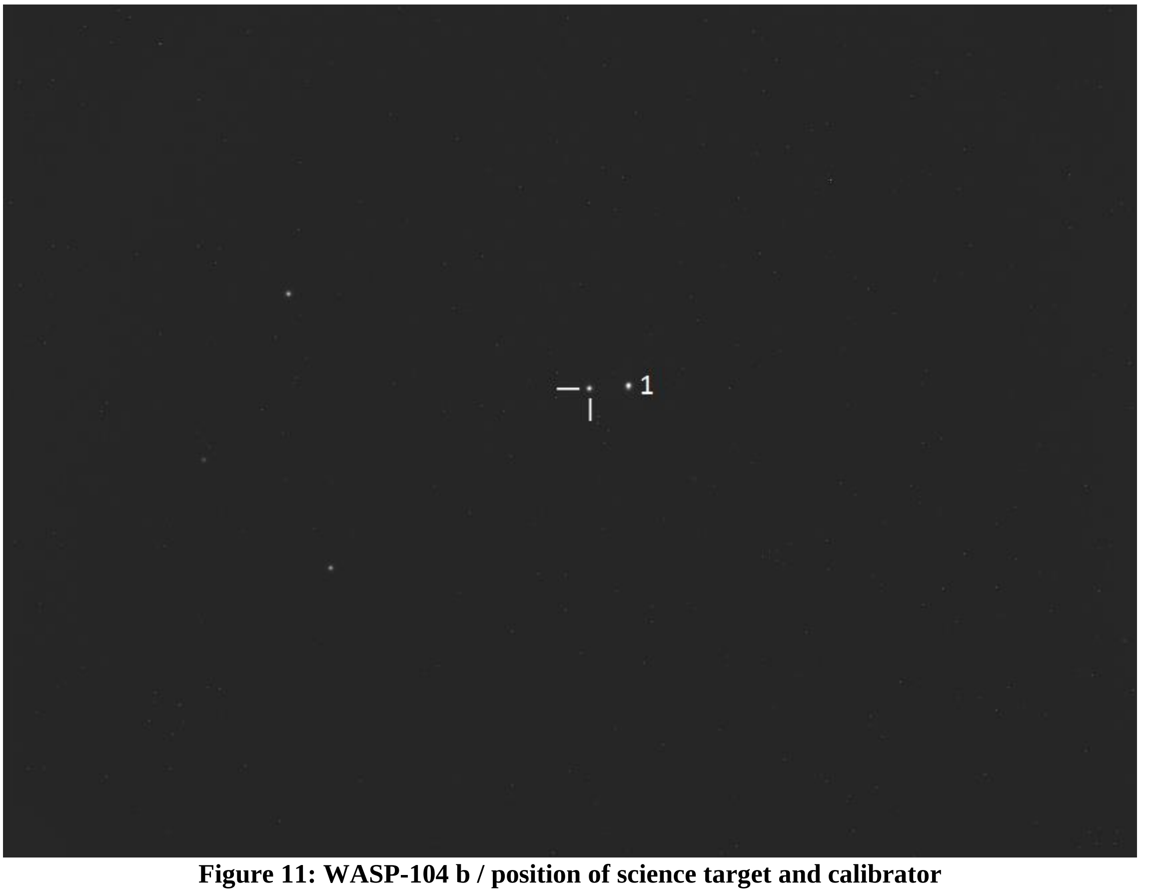

Figure 11: WASP-104 b / position of science target and calibrator

In Figures 11,13,15,16 and 18 the field of view received from the telescope and registered by the CCD detector is displayed. The observed science target is indicated by the horizontal and vertical white lines. The calibrators are marked with numbers.

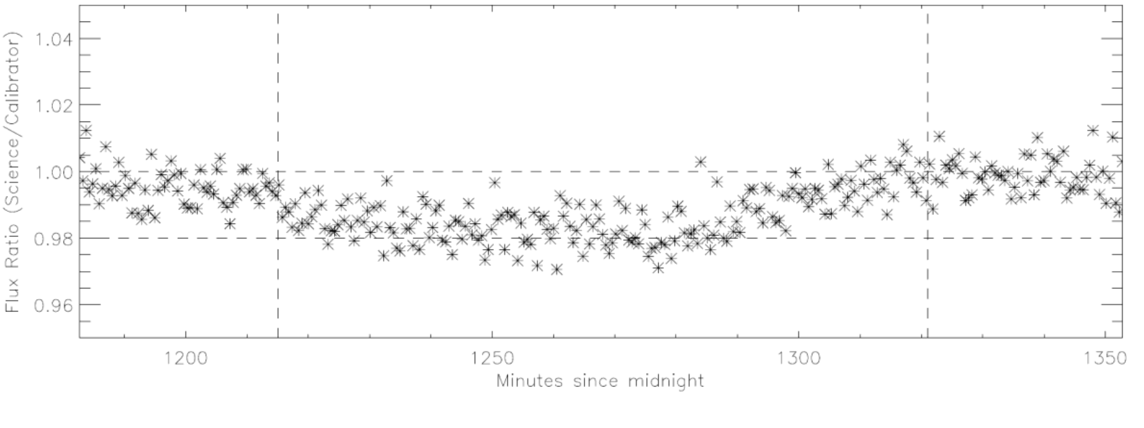

Figure 12: WASP-104 b: flux ratio during transit event

Figure 12 shows the flux ratio between the science target WASP-104 b and the calibrator. Ideally, the calibrator star shows no variability leading to a constant flux as a reference to the science target. The transiting exoplanet disturbs this constant ratio (in the above figure normalized) resulting in the dip in the light curve. On the x-axis the time in minutes that has passed since midnight is shown and the flux ratio is presented on the y-axis. Each flux measurement is marked with a star symbol. The upper horizontal, dashed line indicates the normalized lux ratio. The lower dashed line serves as a guideline in order to make it easier to determine the decrease in flux. The two vertical, dashed lines mark the predicted start and end of the transit. In the field of view there are more stars visible than the science target and one calibrator. The reason why those are not dealt with as calibrators is that a calibrator is required to be similar in flux to the observed star. Most of the stars are fainter and therefore unsuitable for the analysis. Stars brighter than the science target often fall in the non-linear regime of the camera or are even saturated.

With regard to the exoplanet WASP-104 b, the weather conditions allowed an undisturbed observation reflected in the significantly visible transit in the light curve. A computational defect in the automated tracking system of the dome represented the only and minor problem during the transit event, making manual adjustments of the dome necessary.

This monitoring results in a measured transit depth of about 1.5 %. It is assumed that prior to and after the transit the flux ratio is $\mathrm{F_2} = 0.995$ and at the lowest point it is $\mathrm{F_1} = 0.980$. The flux is associated with the apparent magnitude prior and during the transit as follows:

$$\mathrm{m_1 - m_2} = -2.5 \log\left(\frac{\mathrm{F_1}}{\mathrm{F_2}}\right) \tag{13}$$

$$-2.5 \log\left(\frac{0.980}{0.995}\right) = 0.0165 \text{ mag} \tag{14}$$

In this case the calculated difference in apparent magnitude matches the predicted depth of 0.0158 mag by the Czech Exoplanet Transit Database (ETD) quite nicely. This result shows clearly that small differences in magnitude are very similar to the relative decrease in flux.

The radius of host star WASP-104 is $\mathrm{R_*} = (0.963 \pm 0.027)\ \mathrm{R_{sol}}$ (EDE, 2016). By using Formula (8), the radius of the transiting planet is calculated in the following way:

$$\mathrm{R_P} = \sqrt{\frac{\Delta \mathrm{F}}{\mathrm{F}} \mathrm{R_*^2}} = \sqrt{\frac{0.015}{0.995} \cdot (0.963\ \mathrm{R_{Sol}})^2} = 0.118\ \mathrm{R_{Sol}} \tag{15}$$

To get a first impression of the errors, the Gaussian error propagation was applied:

$$\Delta \mathrm{R_P} = \sqrt{\left(\left|\frac{\partial \mathrm{R_P}}{\partial \mathrm{R_*}}\right| \cdot \Delta R_*\right)^2} = \sqrt{\frac{\Delta \mathrm{F}}{\mathrm{F}}} \cdot \Delta \mathrm{R_*} = 0.003\ \mathrm{R_{Sol}} \tag{16}$$

The density is then derived with the known mass of the planet with $\rho_\mathrm{P} = \frac{3\mathrm{M_P}}{4\pi \mathrm{R_P^3}}$.

$$\rho_\mathrm{P} = \frac{3 \cdot 1.272\ \mathrm{M_{Jup}}}{4\pi \cdot (0.118\ \mathrm{R_{Sol}})^3} = 1042\ \mathrm{kg/m^3} \tag{17}$$

$$\Delta\rho_P = \sqrt{\left(\left|\frac{\partial\rho_P}{\partial R_P}\right| \cdot \Delta R_P\right)^2 + \left(\left|\frac{\partial\rho_P}{\partial M_P}\right| \cdot \Delta M_P\right)^2}$$

$$= \sqrt{\left(\left|\frac{-9 \cdot M_P}{4\pi \cdot R_P^4}\right| \cdot \Delta R_P\right)^2 + \left(\left|\frac{3}{4\pi \cdot R_P^3}\right| \cdot \Delta M_P\right)^2} = 88 \text{ kg/m}^3 \tag{18}$$

$$R_P = 0.118\ R_{Sol}, \Delta R_P = 0.003\ R_{Sol}, M_P = 1.272\ M_{jup}, \Delta M_P = 0.047\ M_{Jup}$$

Compared to the data offered by NASA Exoplanet Archive, the generated planetary radius and density fall within the uncertainties. The expected values for those properties are $R_P = (0.117 \pm 0.004)\ R_{Sol}$ and $\rho_P = (1074 \pm 88)\ \text{kg/m}^3$. This observation results in $R_P = (0.118 \pm 0.003)\ R_{Sol}$ and $\rho_P = (1042 \pm 88)\ \text{kg/m}^3$.

By analysing the light curve, the estimated duration is 105 min, from 1210 min to 1315 min since midnight. Both, the duration and the depth, correspond well to the predicted data by ETD. The start and end of this observation is merely shifted 5 min forward.

When using Equation (12) with the measured and known data, the inclination of the planetary trajectory is easy to obtain:

$$i = \cos^{-1}\left(\frac{\sqrt{(R_P + R_*)^2 - \left(\sin\left(\frac{\pi t}{P}\right) \cdot a\right)^2}}{a}\right) = 83.46° \tag{19}$$

$$i_{max} = \cos^{-1}\left(\frac{\sqrt{(R_P - \Delta R_P + R_* - \Delta R_*)^2 - \left(\sin\left(\frac{\pi t}{P}\right) \cdot a\right)^2}}{a}\right) = 83.89° \tag{20}$$

$$\Delta i = i_{max} - i = 0.43° \tag{21}$$

$$R_P = 0.118\ R_{Sol}, R_* = 0.963\ R_{Sol}, t = 105\ min, P = 1.755\ days, a = 0.029\ AU$$

In this case the uncertainty of the inclination was estimated using the min-max estimate method, just because it is much more convenient than the Gaussian error propagation. The corresponding value in literature is $i = (83.63 \pm 0.25)°$. The calculation results in $i = (83.46 \pm 0.43)°$ which represents a satisfactory solution.

It has been proved that the exoplanet WASP-104 b can be detected by using the transit method and the data given by ETD and the NASA Exoplanet Archive could be reproduced in an adequate manner.

3.3 HAT-P-12 b

Located in the constellation Canes Venatici the exoplanet HAT-P-12 b represented the science target of March 20th, 2016. The orbital period around the star of spectral type K4 is 3.213 days. The planet shows a Jupiter-like radius but has only (0.211 ± 0.013) Jupiter masses. The semi-major axis is about 0.038 AU. (EDE, 2016)

Table 4: Event data HAT-P-12 b (ETD, 2016)

Name	HAT-P-12 b (CVn)
RA (J2000)	13:57:33.684 (h:m:s)
DE (J2000)	+ 43:29:37.35 (d:m:s)
Magnitude	12.8 mag
Depth	0.0204 mag
Duration	140.3 min
Predicted start	20:10 UT
Predicted end	22:30 UT
Start of observation	19:41 UT
End of observation	22:58 UT
Elevation	(41-64) °
Exposure time	1.5 min
Focus	4.25 mm
Filter	R
Binning	2x2

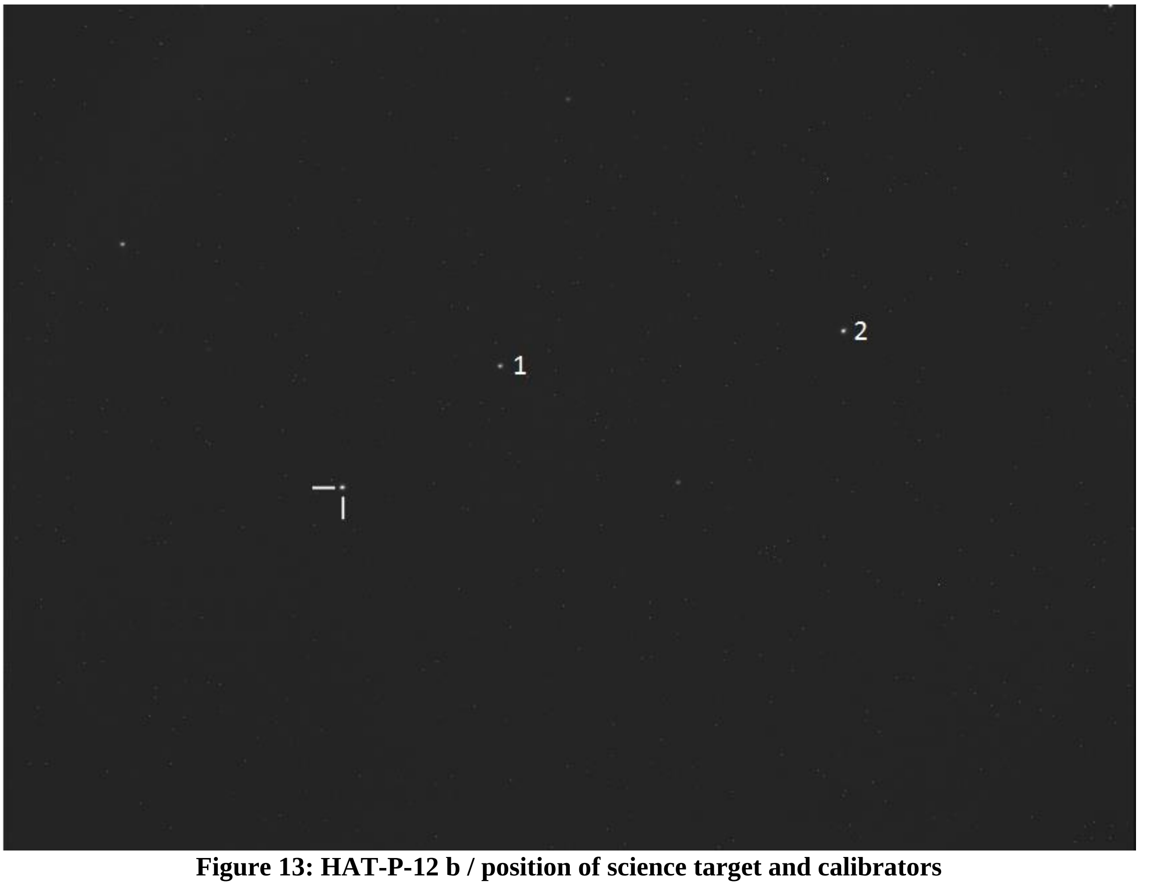

Figure 13: HAT-P-12 b / position of science target and calibrators

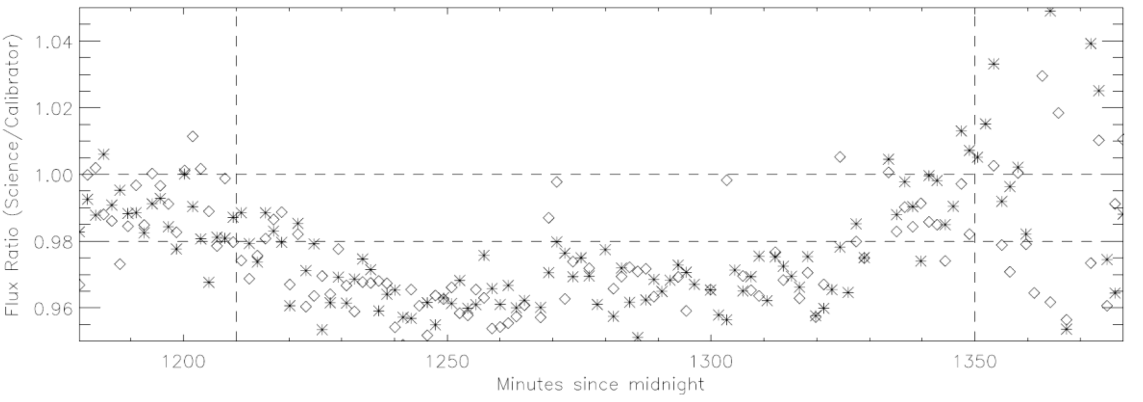

Figure 14: HAT-P-12 b: flux ratio during transit event

Figure 14 shows the flux ratio between the science target HAT-P-12 b and the two calibrators. Each measured flux ratio is marked with a star or diamond symbol according to the used calibrator. Again, the two vertical, dashed lines mark the predicted start and end of the transit. This time more than one calibrator is used in order to generate another light curve to improve and to check the data.

The weather seemed to be acceptable for a transit observation but unfortunately towards the end of the observation cirrus clouds and low stratus appeared. Moon light might have been reflected at the clouds leading to even more unfavourable conditions. The weather change might explain the noisy light curve at the end of the predicted transit. Worth mentioning as well is the fact that the dome had to be manually adjusted causing a potential shadowing of the telescope. Nevertheless, the depth can be determined to be 2.5 % ($\mathrm{F_1} = 0.965, \mathrm{F_2} = 0.990$). Furthermore, the difference in the apparent magnitude is given as follows:

$$-2.5 \log\left(\frac{0.965}{0.990}\right) = 0.0278 \text{ mag} \qquad (22)$$

In this case the calculated difference in apparent magnitude differs from the predicted depth of 0.0204 mag (ETD). A possible explanation could be found in the strangely distributed measurement at the end of the observation. Therefore, the determination of a flux value was difficult.

The radius of host star HAT-P-12 is $\mathrm{R_*} = (0.701 \pm 0.017)\ \mathrm{R_{sol}}$ (EDE, 2016). The radius of the transiting planet is calculated in the following way:

$$\mathrm{R_P} = \sqrt{\frac{0.025}{0.990} \cdot (0.701\ \mathrm{R_{Sol}})^2} = 0.111\ \mathrm{R_{Sol}} \qquad (23)$$

$$\Delta \mathrm{R_P} = \sqrt{\left(\left|\frac{\partial \mathrm{R_P}}{\partial \mathrm{R_*}}\right| \cdot \Delta R_*\right)^2} = \sqrt{\frac{\Delta \mathrm{F}}{\mathrm{F}}} \cdot \Delta \mathrm{R_*} = 0.003\ \mathrm{R_{Sol}} \qquad (24)$$

The density is then derived:

$$\rho_P = \frac{3 \cdot 0.211\ \mathrm{M_{Jup}}}{4\pi \cdot (0.111\ \mathrm{R_{Sol}})^3} = 208\ \mathrm{kg/m^3} \tag{25}$$

$$\Delta\rho_P = \sqrt{\left(\left|\frac{\partial\rho_P}{\partial R_P}\right| \cdot \Delta R_P\right)^2 + \left(\left|\frac{\partial\rho_P}{\partial M_P}\right| \cdot \Delta M_P\right)^2}$$
$$= \sqrt{\left(\left|\frac{-9 \cdot \mathrm{M_P}}{4\pi \cdot \mathrm{R_P^4}}\right| \cdot \Delta R_P\right)^2 + \left(\left|\frac{3}{4\pi \cdot \mathrm{R_P^3}}\right| \cdot \Delta M_P\right)^2} = 21\ \mathrm{kg/m^3} \tag{26}$$

$$R_P = 0.111\ R_{Sol}, \Delta R_P = 0.003\ R_{Sol}, M_P = 0.211\ M_{jup}, \Delta M_P = 0.013\ M_{Jup}$$

The expected values according to NASA Exoplanet Archive and EDE for those properties are $\mathrm{R_P} = (0.099 \pm 0.003)\ \mathrm{R_{Sol}}$ and $\rho_P = (295 \pm 25)\ \mathrm{kg/m^3}$. This observation results in $\mathrm{R_P} = (0.111 \pm 0.003)\ \mathrm{R_{Sol}}$ and $\rho_P = (208 \pm 21)\ \mathrm{kg/m^3}$.

The duration of 140 min, from 1200 min to 1340 min since midnight, corresponds well to the predicted data. This time the start and end of this observation is merely shifted 10 min forward.

The inclination of the planetary trajectory is further obtained:

$$i = \cos^{-1}\left(\frac{\sqrt{(R_P + R_*)^2 - \left(\sin\left(\frac{\pi t}{P}\right) \cdot a\right)^2}}{a}\right) = 88.36° \tag{27}$$

$$i_{max} = \cos^{-1}\left(\frac{\sqrt{(R_P - \Delta R_P + R_* - \Delta R_*)^2 - \left(\sin\left(\frac{\pi t}{P}\right) \cdot a\right)^2}}{a}\right) = 88.94\ ° \tag{28}$$

$$\Delta i = i_{max} - i = 0.58\ ° \tag{29}$$

$$R_P = 0.111\ R_{Sol}, R_* = 0.701\ R_{Sol}, t = 140\ min, P = 3.213\ days, a = 0.038\ AU$$

Thus, the calculations lead to $i = (88.36 \pm 0.58)°$. The corresponding value in literature is $i = (89.0 \pm 0.4)°$. Again, the result turns out to match the given value quite accurately.

The transit of the planet HAT-P-12 b is verified and the determined values are reasonable.

3.4 EPIC-211089792 b

Also known as K2-29 b or WASP-152 b, this exoplanet orbits in 3.259 days around a relatively bright G7 dwarf at a distance of 0.042 AU. It was the target on March 30th, 2016. This planet found in the Taurus constellation resembles Jupiter in radius but has (0.73 ± 0.04) Jupiter masses. The hot Jupiter's parent star has a nearby K5V companion which makes it a binary system. (Santerne et al., 2016)

Table 5: Event data EPIC-211089792 b (ETD, 2016)

Name	EPIC-211089792 b (Tau)
RA (J2000)	04:10:40.955 (h:m:s)
DE (J2000)	+ 24:24:07:35 (d:m:s)
Magnitude	12.526 mag
Depth	0.0215 mag
Duration	133.2 min
Predicted start	18:09 UT
Predicted end	20:22 UT
Start of observation	18:18 UT
End of observation	20:42 UT
Elevation	(42-20) °
Exposure time	10x: 1 min 2x: 1.5 min until 19:45 UT: 2 min until end: 2.5 min
Focus	4.25 mm
Filter	R
Binning	2x2

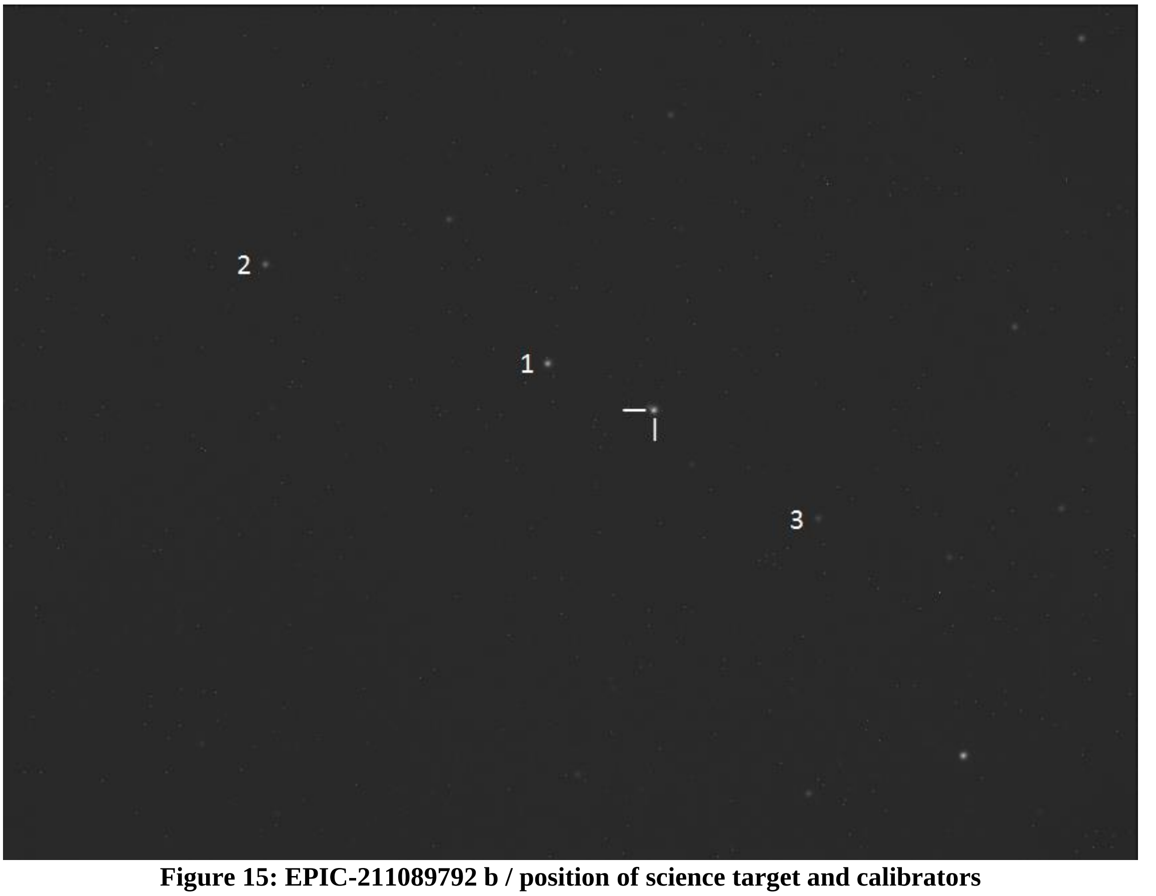

Figure 15: EPIC-211089792 b / position of science target and calibrators

Figure 15 shows the field of view of the observation of EPIC-211089792 b. When studying the science target more closely, one can tell that there is a second star nearby the brighter host star on the right. Therefore, a binary system was observed.

Unfortunately, the transit event of the extrasolar planet EPIC-211089792 b has to be announced as failed. No reasonable light curve could be extracted from the collected data. Many factors played a role in the unmanageable difficulties of the observation. First of all, the decreasing elevation significantly changed the flux of the science target in the course of the event. The exposure time had to be changed multiple times in response to the rapid decrease in the count rate. At the end of the observation the elevation of about 20 ° also pushed the pointing of the telescope to its limits. Due to the early transit start, the beginning of the event could not be recorded because the sky was still too bright at that time. All these unfavourable conditions led to the failure in demonstrating that the transit of this exoplanet exists. See Figure 23 for the non-physical solution.

3.5 XO-1 b

The solar-like star XO-1 hosts the eponymous planet XO-1 b found in the constellation Corona Borealis. 172 pc from Earth this hot Jupiter completes its orbit in 3.942 days and was observed on March 30th, 2016. The exoplanet shows (0.918 ± 0.079) Jupiter masses. The semi-major axis is about 0.049 AU. (EDE, 2016)

Table 6: Event data XO 1 b (ETD, 2016)

Name	XO-1 b (CrB)
RA (J2000)	16:02:12 (h:m:s)
DE (J2000)	+ 28:10:11 (d:m:s)
Magnitude	11.3 mag
Depth	0.0171 mag
Duration	179.5 min
Predicted start	21:40 UT
Predicted end	00:39 UT
Start of observation	21:05 UT
End of observation	01:00 UT
Elevation	(33-62) °
Exposure time	till 22:40 UT: 1 min 5x: 2 min. until 23:48 UT: 1 min until end: 0.75 min
Focus	4.25 mm
Filter	R
Binning	2x2

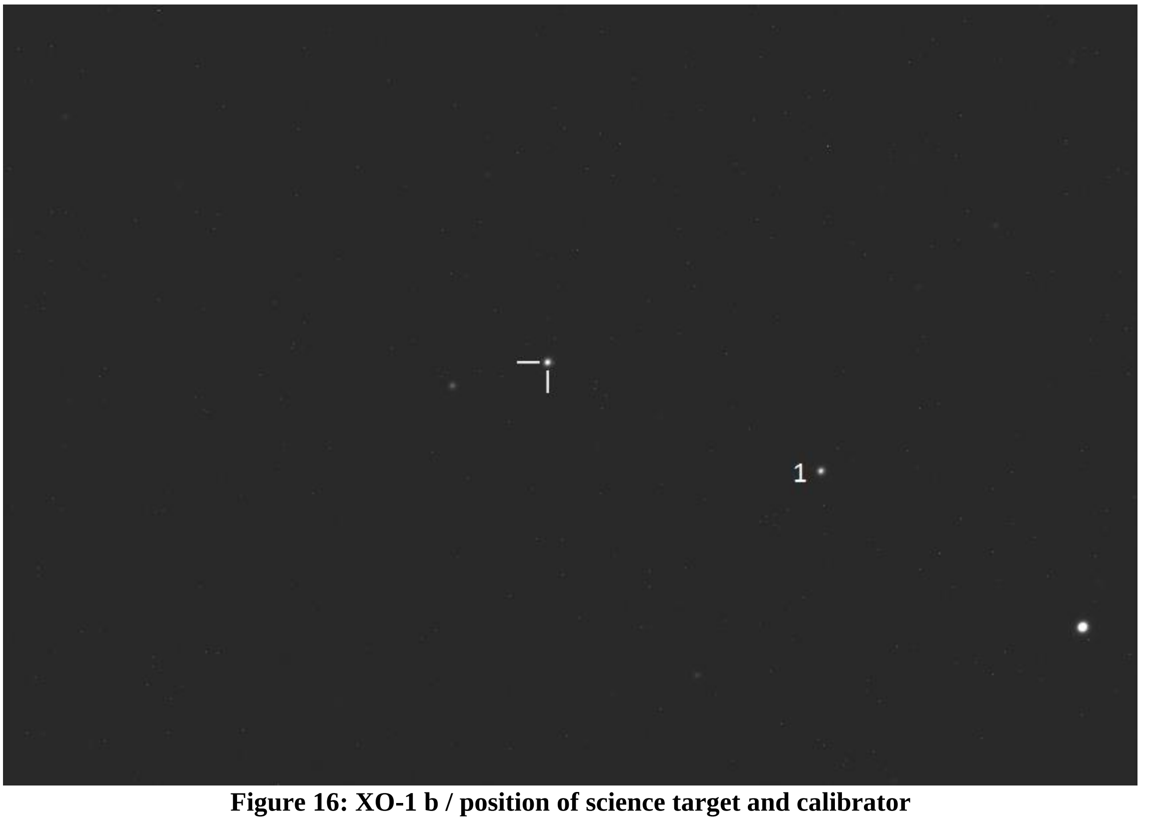

Figure 16: XO-1 b / position of science target and calibrator

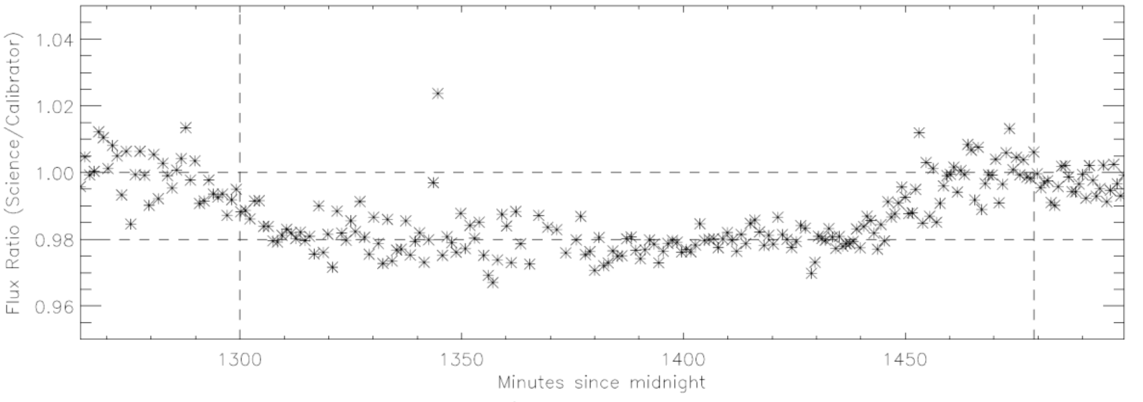

Figure 17: XO-1 b: flux ratio during transit event

Figure 17 shows the flux ratio of the science target XO-1 b and the calibrator. In the field of view, a bright star appears on the bottom right. As mentioned earlier, not all visible stars can be used as calibrators. This one was saturated during the whole observation.

A clear, extremely dark sky and an ascending star are optimal circumstances for this observation. Nevertheless, there was a vivid decrease in the count rate forcing multiple adjustments of the exposure time. One explanation for this phenomenon might be condensation trails and thin cirrus clouds. Still, the evidence for a transit event is clearly visible in the light curve. The steep part on the right represents the exit of the transiting planet ideally. The transit depth is estimated to be about 1.5 % ($\mathrm{F_1} = 0.980, \mathrm{F_2} = 0.995$). The flux is associated with the apparent magnitude prior and during the transit as follows:

$$-2.5 \log\left(\frac{0.980}{0.995}\right) = 0.0165 \text{ mag} \tag{30}$$

In this case the difference in apparent magnitude is expected to be 0.0171 mag.

The radius of host star XO-1 is $\mathrm{R_*} = (0.942 \pm 0.024)\ \mathrm{R_{sol}}$ (NASA Exoplanet Archive, 2016). By using Equation (8), the radius of the transiting planet is calculated in the following way:

$$\mathrm{R_P} = \sqrt{\frac{0.015}{0.995} \cdot (0.934\ \mathrm{R_{Sol}})^2} = 0.115\ \mathrm{R_{Sol}} \tag{31}$$

$$\Delta \mathrm{R_P} = \sqrt{\left(\left|\frac{\partial \mathrm{R_P}}{\partial \mathrm{R_*}}\right| \cdot \Delta R_*\right)^2} = 0.005\ \mathrm{R_{Sol}} \tag{32}$$

The density is further given as:

$$\rho_P = \frac{3 \cdot 0.918\ M_{Jup}}{4\pi \cdot (0.115\ R_{Sol})^3} = 812\ kg/m^3 \tag{33}$$

$$\Delta\rho_P = \sqrt{\left(\left|\frac{\partial\rho_P}{\partial R_P}\right| \cdot \Delta R_P\right)^2 + \left(\left|\frac{\partial\rho_P}{\partial M_P}\right| \cdot \Delta M_P\right)^2} = 127\ kg/m^3 \tag{34}$$

$$R_P = 0.115\ R_{Sol}, \Delta R_P = 0.005\ R_{Sol}, M_P = 0.918\ M_{jup}, \Delta M_P = 0.079\ M_{Jup}$$

This observation results in $R_P = (0.115 \pm 0.005)\ R_{Sol}$ and $\rho_P = (812 \pm 126)\ kg/m^3$. Compared to the data offered by EDE, the generated planetary radius and density are acceptable when taking the uncertainty into account. The expected values for those properties are $R_P = (0.121 \pm 0.005)\ R_{Sol}$ and $\rho_P = (650 \pm 96)\ kg/m^3$.

An astonishing fact is the shift in the transit time. This observation suggests a start and end 15 min prior to the predicted time (from 1285 to 1460 min since midnight). This results in a duration of 175 min, a difference of 5 min to the data by ETD.

The inclination of the planetary trajectory is calculated below:

$$i = \cos^{-1}\left(\frac{\sqrt{(R_P + R_*)^2 - \left(\sin\left(\frac{\pi t}{P}\right) \cdot a\right)^2}}{a}\right) = 88.52\ ° \tag{35}$$

$$i_{max} = \cos^{-1}\left(\frac{\sqrt{(R_P - \Delta R_P + R_* - \Delta R_*)^2 - \left(\sin\left(\frac{\pi t}{P}\right) \cdot a\right)^2}}{a}\right) = 89.36\ ° \tag{36}$$

$$\Delta i = i_{max} - i = 0.84\ ° \tag{37}$$

$$R_P = 0.115\ R_{Sol}, R_* = 0.942\ R_{Sol}, t = 175\ min, P = 3.942\ days, a = 0.049\ AU$$

The corresponding value in literature is $i = (88.8 \pm 0.7)°$ (EDE, 2016). The computation of the inclination using the data obtained by the observation leads to $i = (88.52 \pm 0.84)°$. Ones more the given value could be replicated satisfactory.

Evidence for the transiting planet XO-1 b has been found and the data offered by EDE was confirmed.

3.6 HAT-P-5 b

On May 5th, 2016 a clear, cloudless sky offered the perfect conditions to observe the extrasolar planet HAT-P-5 b in the constellation Lyra. 340 pc from Earth, this hot Jupiter orbits its Sun-like host star in 2.788 days and has (1.060 ± 0.113) Jupiter masses. The semi-major axis is 0.041 AU. (EDE, 2016)

Table 7: Event data HAT-P-5 b (ETD, 2016)

Name	HAT-P-5 b (Lyr)
RA (J2000)	18:17:37.3 (h:m:s)
DE (J2000)	+ 36:37:16.6 (d:m:s)
Magnitude	12 mag
Depth	0.0142 mag
Duration	175 min
Predicted start	19:50 UT
Predicted end	22:45 UT
Start of observation	19:36 UT
End of observation	23:11 UT
Elevation	(31-61) °
Exposure time	1 min
Focus	4.25 mm
Filter	R
Binning	2x2

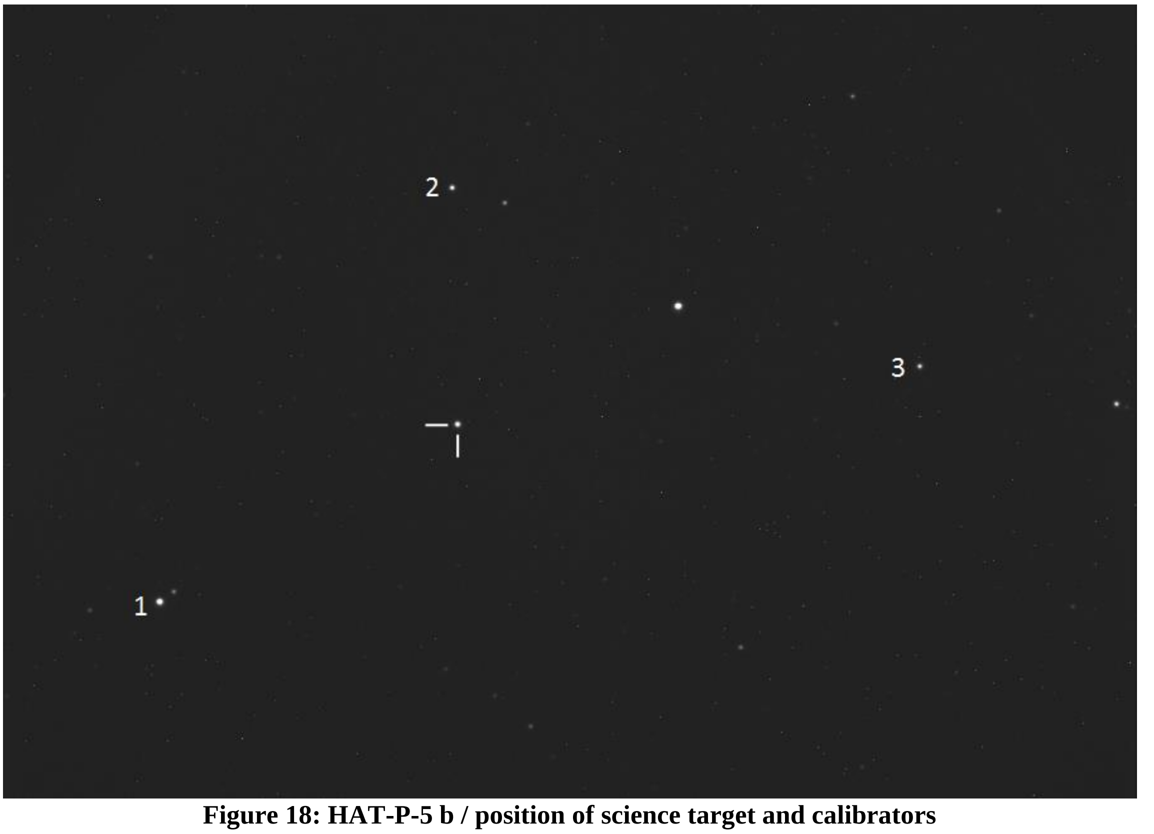

Figure 18: HAT-P-5 b / position of science target and calibrators

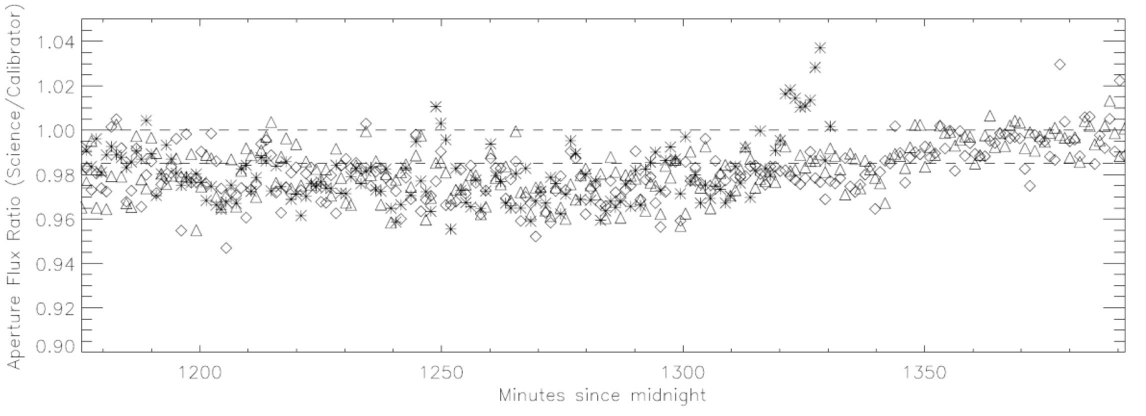

Figure 19: HAT-P-5 b: flux ratio during transit event

Three surrounding stars in this field of view were appropriate to be used as calibrators. The measurements are marked with star, triangle and diamond symbols. Although the dots seem to be arranged randomly on first sight, the dip in the flux ratio in the middle is clearly visible when comparing the right end of the graph with the centre. For more details about aperture photometry see Figure 20.

A cloudless sky offered perfect circumstances for the final transit event in the course of five observations. One day prior to full moon the light of the Earth's companion might, however, play a role. A slight rise in the count rate towards the end was recorded.

It is clearly visible that the dip in the light curve is not as clear as the others before but it is rated to be about 2 %. It is assumed that prior to and after the transit the flux ratio is $\mathrm{F}_2 = 0.995$ and at the lowest point it is $\mathrm{F}_1 = 0.975$. The apparent magnitude changes by:

$$-2.5\log\left(\frac{0.975}{0.995}\right) = 0.0220\ \mathrm{mag} \tag{38}$$

ETD suggests a depth of 0.0142 mag which significantly differs from the calculation.

The radius of host star HAT-P-5 is $\mathrm{R}_* = (1.165 \pm 0.052)\ \mathrm{R}_{\mathrm{sol}}$ (EDE, 2016). The planetary radius is given as:

$$\mathrm{R}_\mathrm{P} = \sqrt{\frac{0.02}{0.995} \cdot (1.165\ \mathrm{R}_{\mathrm{Sol}})^2} = 0.165\ \mathrm{R}_{\mathrm{Sol}} \tag{39}$$

$$\Delta\mathrm{R}_\mathrm{P} = \sqrt{\left(\left|\frac{\partial \mathrm{R}_\mathrm{P}}{\partial \mathrm{R}_*}\right| \cdot \Delta R_*\right)^2} = \sqrt{\frac{\Delta\mathrm{F}}{\mathrm{F}}} \cdot \Delta\mathrm{R}_* = 0.007\ \mathrm{R}_{\mathrm{Sol}} \tag{40}$$

The density is derived as $\rho_P = \frac{3M_P}{4\pi R_P^3}$.

$$\rho_P = \frac{3 \cdot 1.060\ M_{Jup}}{4\pi \cdot (0.165\ R_{Sol})^3} = 317\ kg/m^3 \tag{41}$$

$$\Delta\rho_P = \sqrt{\left(\left|\frac{\partial\rho_P}{\partial R_P}\right| \cdot \Delta R_P\right)^2 + \left(\left|\frac{\partial\rho_P}{\partial M_P}\right| \cdot \Delta M_P\right)^2} = 53\ kg/m^3 \tag{42}$$

$$R_P = 0.165\ R_{Sol}, \Delta R_P = 0.007\ R_{Sol}, M_P = 1.060\ M_{jup}, \Delta M_P = 0.113\ M_{Jup}$$

$R_P = (0.130 \pm 0.005)\ R_{Sol}$ and $\rho_P = (660 \pm 120)\ kg/m^3$ are the corresponding values in literature (NASA Exoplanet Archive, 2016). The observation suggests a planetary radius of $R_P = (0.165 \pm 0.007)\ R_{Sol}$ and a density of $\rho_P = (317 \pm 53)\ kg/m^3$.

Due to a late start of the observation it is hard to tell when exactly the graph begins to decrease. But taking the origin of the light curve at 1175 min since midnight and an estimated end at 1355 min since midnight (180 min in total), there is only a time difference of 5 min with regard to the predicted duration of 175 min. The observed transit is shifted 10 min forward.

The inclination of the planetary trajectory is calculated by applying Formula (12):

$$i = \cos^{-1}\left(\frac{\sqrt{(R_P + R_*)^2 - \left(\sin\left(\frac{\pi t}{P}\right) \cdot a\right)^2}}{a}\right) = 86.89\ ° \tag{43}$$

$$i_{max} = \cos^{-1}\left(\frac{\sqrt{(R_P - \Delta R_P + R_* - \Delta R_*)^2 - \left(\sin\left(\frac{\pi t}{P}\right) \cdot a\right)^2}}{a}\right) = 88.14\ ° \tag{44}$$

$$\Delta i = i_{max} - i = 1.25\ ° \tag{45}$$

$$R_P = 0.165\ R_{Sol}, R_* = 1.165\ R_{Sol}, t = 180\ min, P = 2.788\ days, a = 0.041\ AU$$

The corresponding value in literature is $i = (86.75 \pm 0.44)°$ (NASA Exoplanet Archive, 2016). The calculations suggest a value of $i = (86.89 \pm 1.25)°$.

A transit of the exoplanet HAT-P-5 b is not questioned. The predicted data could be replicated in an adequate manner.

4 Conclusion

Extrasolar planets exist in many variations around different stars. The search for exoplanets looks back to a rapid progress in theoretical and experimental research. The number of discovered and later confirmed bodies in diverse systems is continuously increasing due to a tremendous development of detection methods and instruments. Compared to our Solar system, some features are also found in extrasolar systems like planetary types (terrestrial or Jovian) or low eccentricities. In contrary, some conditions were new to scientists (hot Jupiters). The hunt for an Earth-like planet capable of hosting some form of life is still a hot topic for researchers and far from being completed.

It is proved that by using the instruments at the observatory Lustbühel in Graz a transit event can be detected. For four out of five observations it was possible to generate a light curve indicating a clear dimming in the star's light due to a transiting planet. Therefore, the survey was a great success. This technique, however, is quite sensitive to bad conditions like cirrus clouds and moon light. Precise adjustments need to be done to grant the required precision and reduce any form of uncertainties.

Generally speaking, the data received and further analysed agrees with the predicted values by either the Exoplanet Transit Database, NASA Exoplanet Archive or Exoplanet Data Explorer. Reasons for any deviations might be subsequent errors made by analysing the light curve and further calculating the properties with this data. The instruments are very sensitive to disturbances generated by for instance weather changes or moon light. In the previous chapter the determination of the flux ratio prior and during the transit is estimated by the observer, but is normally fitted with mathematical methods. On the basis of this value the planetary radius and density as well as the orbital inclination were computed. Thereby, a previously made error could influence the whole analysis.

Table 8: Results of the four successful observations

	WASP-104 b		HAT-P-12 b	
	Observation	Literature	Observation	Literature
Depth / mag	0.0165	0.0158	0.0278	0.0204
Duration / min	105	105.72	140	140.3
R_P / R_{Sol}	0.118 ± 0.003	0.117 ± 0.004	0.111 ± 0.003	0.099 ± 0.003
ρ_P / kg/m³	1042 ± 88	1074 ± 88	208 ± 21	295 ± 25
i / °	83.5 ± 0.5	83.6 ± 0.3	88.4 ± 0.6	89.0 ± 0.4
	XO-1 b		**HAT-P-5 b**	
	Observation	Literature	Observation	Literature
Depth / mag	0.0165	0.0171	0.0220	0.0142
Duration / min	175	179.5	180	175
R_P / R_{Sol}	0.115 ± 0.005	0.121 ± 0.005	0.165 ± 0.007	0.130 ± 0.005
ρ_P / kg/m³	812 ± 126	650 ± 96	317 ± 53	660 ± 120
i / °	88.5 ± 0.9	88.8 ± 0.7	86.9 ± 1.3	86.8 ± 0.5

5 List of references

ASA, Cassegrain Telescope (2016). Available online: https://www.optcorp.com/asa-500-mm-f-9-cassegrain-telescope.html [October 3rd, 2016]

Beaulieu, J.-P. et al. (2006): Discovery of a cool planet of 5.5 Earth masses through gravitational microlensing. Nature, 439, 437-440.

COROT, Mission (2016). Available online: https://corot.cnes.fr/en/home-56 [October 3rd, 2016]

Cowley, M. & Hughes, S. (2014). Characterization of transiting exoplanets by way of differential photometry. IOP Publishing Ltd: Physics Education, 49/3.

Deeg, H. (2002). The Transit Method. Available online: http://www.iac.es/proyecto/tep/transitmet.html [October 3rd, 2016]

ESO Science Release 1245 (2012). Lost in Space: Rogue Planet Spotted?. Available online: http://www.eso.org/public/news/eso1245/ [October 3rd, 2016]

ETD - Exoplanet Transit Database (2016). Available online: http://var2.astro.cz/ETD/ [October 3rd, 2016]

EDE - Exoplanet Data Explorer (2016). Available online: http://exoplanets.org/ [October 3rd, 2016]

Haswell, C. A. (2010). Transiting Exoplanets. New York: Cambridge University Press

HATNet (2015). Available online: http://hatnet.org/ [October 3rd, 2016]

Hirano, T. (2014). Measurements of Spin-Orbit Angles for Transiting Systems. Tokyo: Springer Japan

IAU (2006). Resolution B5. Definition of a Planet in the Solar System. Available online: https://www.iau.org/static/resolutions/Resolution_GA26-5-6.pdf [October 3rd, 2016].

Kepler, NASA Mission (2016). Available online: http://kepler.nasa.gov/ [October 3rd, 2016].

Lammer, H. et al. (2009). What makes a planet habitable?. Astron. Astrophys. Rev. 17, 226-228

Lunine, J. I., Macintosh, B. & Peale S. (2009). The detection and characterization of exoplanets. Physics Today, 62, 46.

Mason, J. W. (2008). Exoplanets. Detection, Formation, Properties, Habitability. Chichester: Praxis Publishing Ltd.

Mayor, M. & Queloz, D. (1995). A Jupiter-mass companion to a solar-type star. Nature, 378, 355-359.

NASA Exoplanet Archive (2016). Available online: http://exoplanetarchive.ipac.caltech.edu/ [October 3rd, 2016].

Perryman, M. (2011). The Exoplanet Handbook. New York: Cambridge University Press.

Piper, S. (2014). Exoplaneten. Die Suche nach einer zweiten Erde. 2nd edition. Heidelberg: Springer Spektrum.

Santerne, A. et al. (2016). K2-29 b/WASP-152 b: An aligned and inflated hot Jupiter in a young visual binary. The Astrophysical Journal, Vol. 824, Nr. 1

Waldmann, I. (2014). L10: Finding exoplanets with Astrometry and Radial velocities. Available online: http://zuserver2.star.ucl.ac.uk/~ingo/Lecture_Notes_files/lect10.pdf [October 3rd, 2016].

WASP, Mission (2014). Available online: http://www.superwasp.org/ [October 3rd, 2016].

Wolszczan, A. & Frail, D. A. (1992). A planetary system around the millisecond pulsar PSR1257+12. Nature, 355, 145-147

6 Appendix

6.1 WASP-104 b

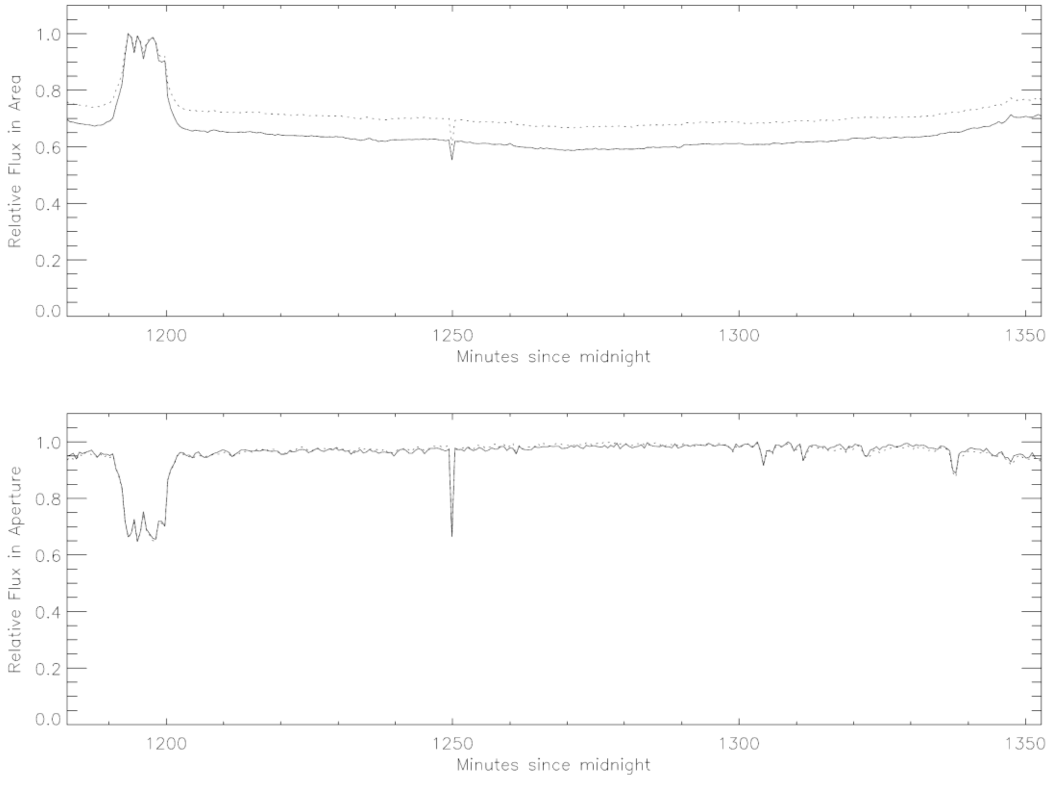

Figure 20: WASP-104 b: Relative flux in area and aperture

In Figure 20 the upper panel shows the relative flux in the area cut out by the data reduction. The measurements of the science target are represented by the black line and the ones of the calibrators are shown by the dotted line. In the analysis, both objects were cut out in a square shape in order to get rid of as much of the surrounding background as possible. To get the flux in the area, the pixel counts within this whole cut-out area were summed for each exposure. To generate the graph, the flux of each image at a specific time since midnight was set into relation to the maximal sum of the series. In aperture photometry (lower panel), the pixel counts within an aperture centred on the object were summed up. An inner and outer radius was set to compute from this background sky annulus the background level which is then subtracted from the counts in the aperture around the stars. Again, the graph was normalized.

6.2 HAT-P-12 b

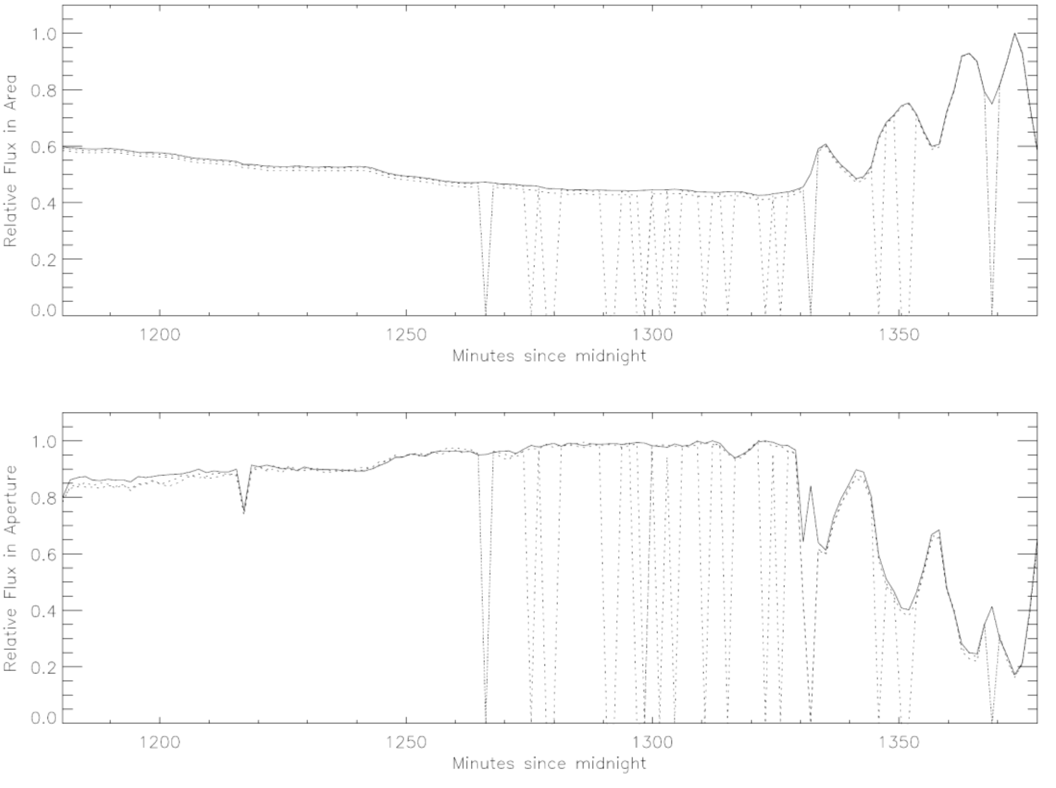

Figure 21: HAT-P-12 b: Relative flux in area and aperture

For more details, see the description of Figure 20.

6.3 EPIC-211089792 b

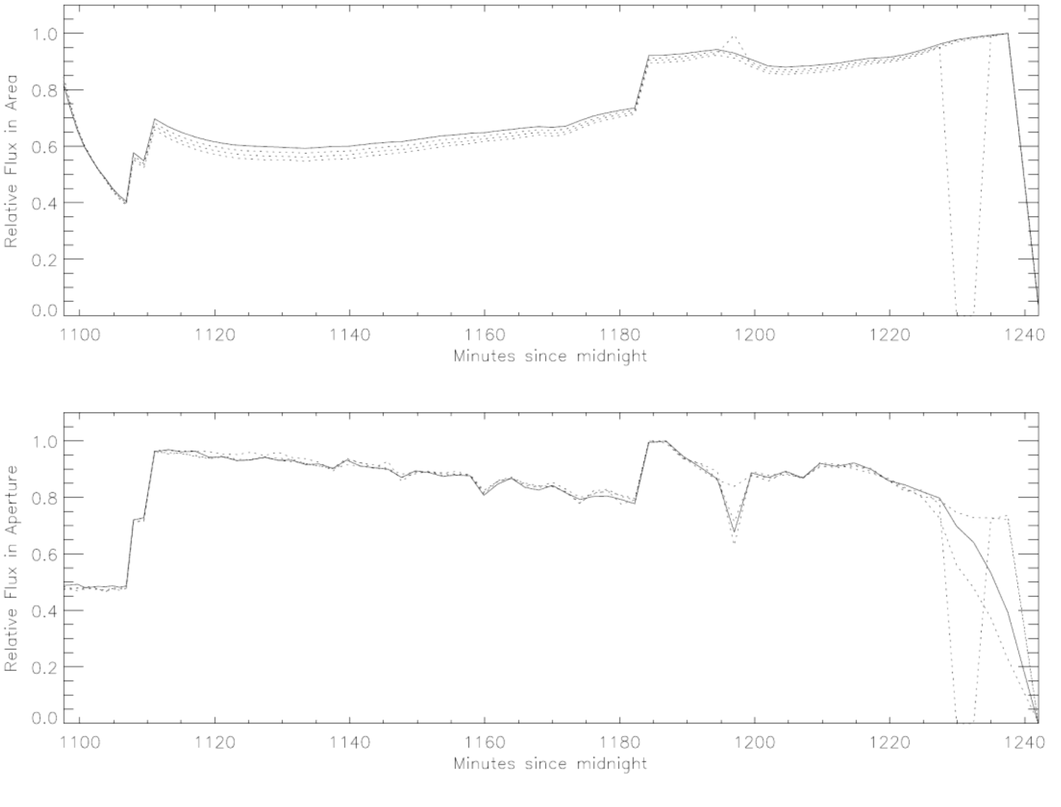

Figure 22: EPIC-211089792 b: Relative flux in area and aperture

For details, see Figure 20. The relative flux in aperture and area is presented in Figure 22. The lines vary significantly indicating that something went wrong.

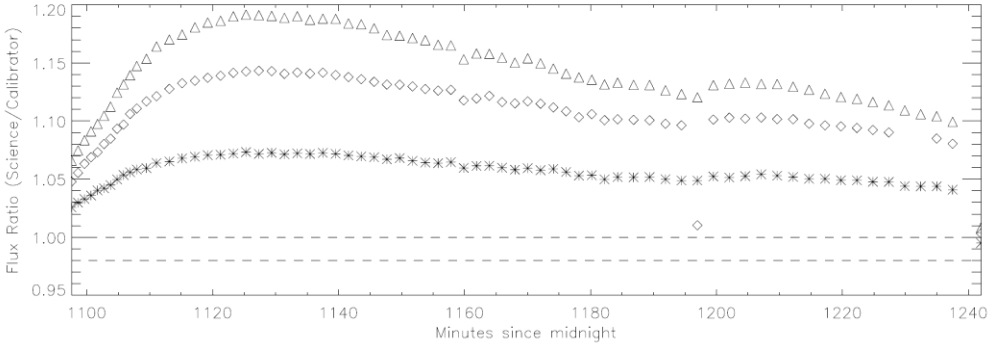

Figure 23: EPIC-211089792 b: flux ratio of star and calibrators during transit event

For a detailed description of the graph, see Figure 12. Unfortunately, it was not possible to generate a reasonable graph showing the desired dip in the light curve. The plot shows non-physical solutions.

6.4 XO-1 b

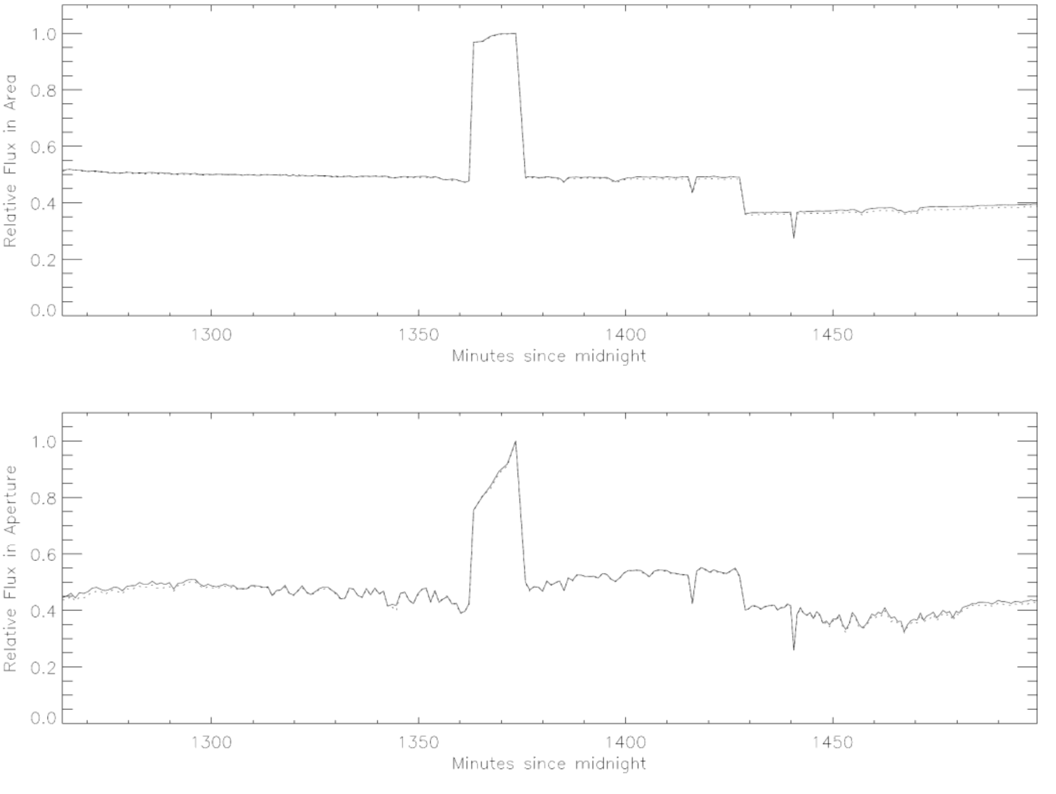

Figure 24: XO-1 b: Relative flux in area and aperture

See Figure 20 for more details concerning the description of the graphs.

6.5 HAT-P-5 b

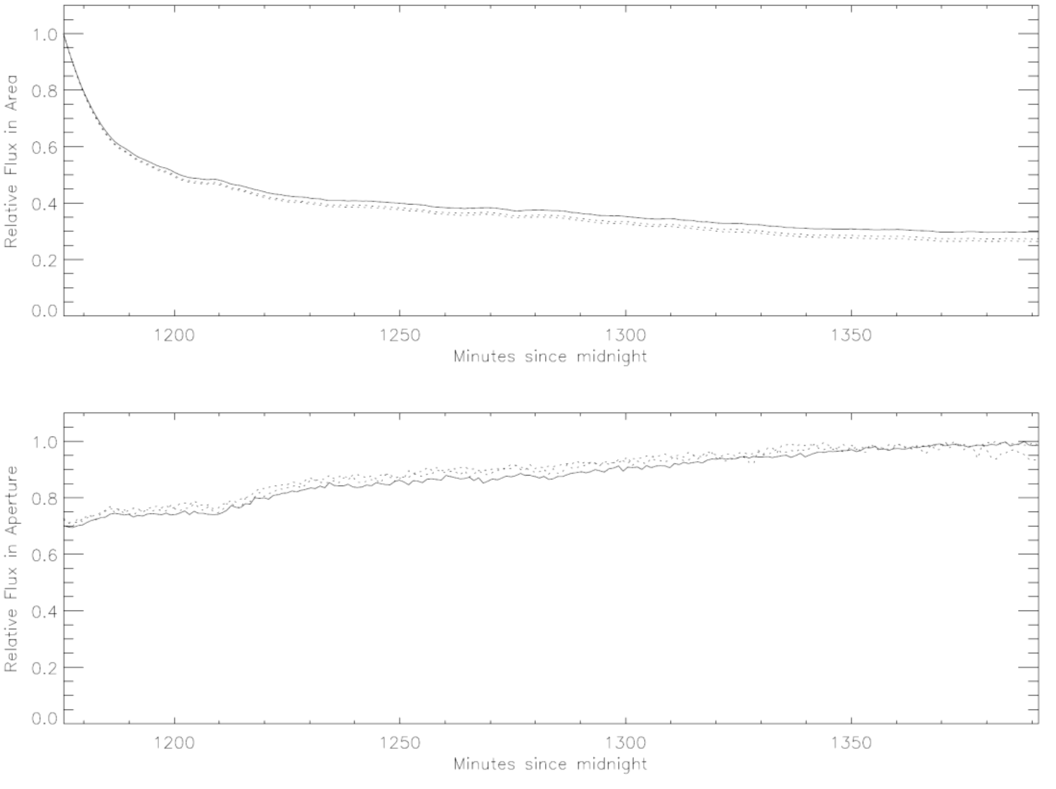

Figure 25: HAT-P-5 b: Relative flux in area and aperture

The description of Figure 20 explains in detail what is shown in Figure 25.